# ALFVÉNIC ACCELERATED ELECTRONS AND SHORT BURST AURORAL KILOMETRIC RADIATIONS OBSERVED BY THE FAST SATELLITE

by

LUN MA

Presented to the Faculty of the Graduate School of

The University of Texas at Arlington in Partial Fulfillment

of the Requirements

for the Degree of

MASTER OF SCIENCE IN PHYSICS

THE UNIVERSITY OF TEXAS AT ARLINGTON

May 2007

To my mother.

## ACKNOWLEDGEMENTS

I would like to thank my supervising professor Dr. Yi-jiun Su for her great support in my research work. Dr. Su was always there to listen, explain and give advice. She taught me how to start and most of the fundamental concepts and skills in doing this research. She read my thesis and answered questions even during her holiday when she was sick. Without her timely guidance, I could not finish this thesis. I also thank professors Dr. James Horwitz and Dr. Manfred Cuntz, for their interest in my research and for taking time to serve in my committee.

I would like to extend my appreciation to Dr. Sam Jones, who helped checking my English in writing academic papers with great conscientiousness. I also say 'thank you' to Jason Eberle and Weichao Wang, who provide many suggestions on utilizing Latex to edit files and figures.

Finally, I thank my family and would like to express my deep gratitude to my wife who take care of my life and give me understanding all the time.

April 20, 2007

## ABSTRACT

ALFVÉNIC ACCELERATED ELECTRONS AND SHORT BURST
AURORAL KILOMETRIC RADIATIONS OBSERVED
BY THE FAST SATELLITE

Publication No. _____

Lun Ma, M.S.

The University of Texas at Arlington, 2007

Supervising Professor: Yi-jiun Su

This investigation is motivated by previous study of short burst radiations (S-bursts) reported by Ergun et al. [2006], who suggested two generation mechanisms of S-bursts: one is the electron cyclotron maser instability due to an unstable ring distribution; the other is an upward electron beam generating upper hybrid resonance. The simulation results reported by Su et al. [2007] support the former mechanism. Only one Earth-based S-burst event was reported prior to our study. A systematic study was performed on particle and field observations from the FAST spacecraft to search for events of S-bursts and Alfvén waves. Eight events involving coexistence were identified and are presented in this thesis. All of them were observed at altitudes greater than 2500 km during winter months. In addition, S-bursts associated with Alfvénic perturbations were detected during periods when the AE indices were high, indicating a possible association with substorms. Furthermore, 24 dayside Alfvénic events and 20 nightside events were examined in detail. We found that the electron phase space density peaks along the

magnetic field line for the nightside, which supports the concept of field-aligned acceleration by inertial Alfvén waves. However, the electron anisotropies involving the phase space densities peaked perpendicular to the magnetic field were observed on the dayside.

## TABLE OF CONTENTS

## LIST OF FIGURES

## LIST OF TABLES

## ABBREVIATIONS

AAR — Auroral Acceleration Region

AKR — Auroral Kilometric Radiation

$B$ — Magnetic field

$B_A$ — Magnetic field at AKR source region

$B_s$ — Magnetic field at satellite location

$\delta B$ — Purterbation of magnetic field

$e$ — Electron charge

$\delta E$ — Purterbation of electric field

$\epsilon_0$ — Permitivity of free space

$F_{\parallel}$ — The peak of the Parallel electron flux ($0^0 - 30^0$ or $150^0 - 180^0$)

$F_{\perp}$ — The peak of the Perpendicular electron flux ($60^0 - 120^0$)

FAST — Fast Auroral SnapshoT

$m$ — Diploe magnetic moment

$m_e$ — Electron mass

$N_{\parallel}$ — Parallel number density in the Northern Hemisphere ($-30^0 \sim 30^0$)

$N_{lc}$ — Loss-cone number density in the Northern Hemisphere ($150^0 \sim 210^0$)

$N_{\perp}$ — Perpendicular number density ($60^0 \sim 120^0$ and $240^0 \sim 300^0$)

PWT — Plasma Wave Tracker

$r$ — Geocentric distance

$r_A$ — Geocentric distance of AKR source region

$r_s$ — Geocentric distance of satellite location

S-burst — Short burst

SFA — Swept Frequency Analysor

$\mu_0$ — Magnetic permibility of free space

$\omega_A$ — Local electron cyclotron frequency at AKR source region or AKR emission frequency

$\omega_s$ — Local electron cyclotron frequency at satellite location

$\omega_{ce}$ — Local electron cyclotron frequency

$\omega_{pe}$ — Plasma frequency

# CHAPTER 1

# INTRODUCTION

The research work presented in this thesis is motivated by previous investigation of short burst radiations reported by Ergun et al. [2006] and Su et al. [2007]. In the first chapter, we begin by introducing Auroral Kilometric Radiation (AKR) and Alfvén waves in Section 1.1, which includes the generation mechanism of AKR. The acceleration aurora region (AAR) can be categorized into three types according to their acceleration mechanisms: (1) the upward current region, (2) the downward current region, and (3) the polar cap boundary acceleration region. They are summarized in Section 1.2. A simply description of the mission of Fast Auroral SnapshoT (FAST) and the data analysis tool are presented in Section 1.3.

## 1.1 Auroral Kilometric Radiation(AKR) and Alfvén waves

### 1.1.1 AKR

Auroral Kilometric Radiation (AKR) is an intense radio emission generated in the Earth's auroral acceleration regions. The frequencies of AKR are typically in the range between 50 and 800 kHz. Beneditkov et al. [1965] first observed this phenomenon as an extra-terrestrial noise with frequency about 1 MHz. Its emission properties were then characterized in the 1970s and early 1980s [Gurnett, 1974; Kurth et al., 1975; Gurnett and Green, 1978; Dusenbery and Lyons, 1982]. When AKR occurs, the total power is about ten megawatts and may occasionally reach gigawatt. The radiation is absorbed by the ionosphere and therefore can only be measured by satellites positioned above the ionosphere.

Unlike the so-called radioactive radiation which is connected with nuclear radioactive processes, AKR is considered as electromagnetic radiation which is related to oscillations of electric and magnetic fields. AKR emission consists of extraordinary-mode waves emitted near the local electron cyclotron frequency, approximately perpendicular to the Earth's magnetic field [Gurnett and Green, 1978; Kaiser et al., 1978; Calvert, 1981a]. Later, Mellott et al. [1984] showed that AKR was mainly "right-hand-X" mode radiation, with a weak "left-hand-O" mode component. From its source region, the AKR emission travels near the speed of the light through the major magnetospheric plasma regions. Hence satellites detect AKR signals within 0.1 millisecond whether they originate hundreds or thousands of kilometers away.

### 1.1.2 The generation mechanism of AKR

Gurnett [1974] and Kurth et al. [1975] found that AKR was generated on auroral field lines where down-going electrons were accelerated, which was then confirmed by Alexander and Kaiser [1976]. One of the first proposed generation mechanisms was a loss-cone instability with a weakly relativistic treatment [Wu and Lee, 1979], which was then coined the electron-cyclotron maser instability by Melrose and Dulk [1982]. However, based on observations from the Viking spacecraft, Louarn et al. [1990] found that the loss-cone instability was insufficient to generate the AKR emissions.

An electron shell distribution is presumably produced by an upward parallel electric field existing at the bottom of a negative potential structure. This type of distribution has been suggested to be more efficient in generating AKR emissions [Pritchett, 1984a, b; Pritchett and Strangeway, 1985; Winglee and Pritchett, 1986; Strangeway et al, 2001]. Based on the data obtained from the FAST satellite, Ergun et al. [1998], Delory et al. [1998] and Strangeway et al. [1998, 2001] suggested that the electron cyclotron maser is

driven by an untable shell distribution. The AKR emissions are believed to be generated by electron maser instability in the auroral density cavity in the upward current region.

The perpendicular-driven instability $\partial f/\partial v_\perp > 0$ (i.e., the positive slope in the electron velocity distribution) is favorable to provide free energy for AKR emissions. This positive slope could be generated in either the loss cone or shell (horseshoe) distributions.

### 1.1.3 Efficient energy conversion

Ergun et al. [2000a] and Pritchett et al. [2002] showed an efficient energy conversion from electron distribution instability to AKR emissions. It requires a very small ratio of electron plasma frequency ($\omega_{pe}$) to electron cyclotron frequency ($\omega_{ce}$), i.e., $\omega_{pe}/\omega_{ce} << 1$, where $\omega_{pe} = \left(e^2 n/m_e\epsilon_0\right)^{1/2}$ and $\omega_{ce} = eB/m_e$. $e$, $n$, $m_e$,$\epsilon_0$ and $B$ are electron charge, plasma density, electron mass, permittivity of free space and magnetic field respectively. The requirement of a lower background plasma density results in a smaller $\omega_{pe}$ and therefore satisfies the efficient energy conversion condition.

Auroral cavities are regions with very low plasma densities. The particle density inside the cavity can be 2 - 3 orders of magnitude lower than typical auroral densities. This is the reason why AKR emissions usually occur in these cavities. Unstable electron shell distributions, the energy source of AKR, have been observed inside the cavities. The size of the auroral cavity is not quantitatively determined. Calvert [1981b] suggested a plasma cavity which extending from 1.3 to at least 3.3 $R_E$ (geocentric radii) at $70^0$ invariant magnetic latitude, in which the plasma density may be less than $1cm^{-3}$. Using observational data and simulations, Ergun et al. [2000b] suggested that the lower boundary of a particlular density cavity is located near 1.6 $R_E$ geocentric distances.

### 1.1.4 Short burst AKR emissions

The short burst radio emissions were first reported in the Jovian decametric emission events by Kraus [1956]. These pulses are narrow-band burst emissions, which reoccur within a few seconds. Recently, Ergun et al. [2006] reported one Earth-based S-burst event which was associated with Alfvén waves during a substorm expansion phase. In addition, Su et al. [2007] suggested that the propagating Alfvén waves may generate unstable electron distributions to trigger short burst emissions.

The main objective of our investigation is to search for additional Earth-based S-burst events which may be associated with Alfvén waves. Characteristics of such events will be discussed in later sections. The ratio of $\omega_{pe}/\omega_{ce}$ on Jupiter is generally about 0.01 but only 0.1 on Earth [Hilgers, 1992]. Ergun et al. and Su et al. indicated that it may be difficult to find S-burst events on Earth due to the higher $\omega_{pe}/\omega_{ce}$ ratio. In this thesis, we report the minimum occurrence frequency of Earth-based S-bursts.

Two possible S-burst growth mechanisms were suggested by Ergun et al. [2006]: (1) a "ring" distribution; and (2) an upward electron beam. It should be noted that the "ring" distribution is referred to as the conic distribution throughout this thesis.

The observation suggests that impulsive electron acceleration and mirroring can create unstable ring distributions [Strangeway et al., 2001]. These distributions are unstable to the electron cyclotron maser, thus the unstable electrons move rapidly away from the planet to produce S-burst emissions. The simulation and data comparison by Su et al. [2007] support the mechanism of the electron cyclotron maser instability.

On the other hand, field-aligned electron fluxes may create a beam-plasma instability which generates oblique waves on upper hybrid resonance cone. Such waves can mode convert to electromagnetic emissions [Budden, 1986; Budden & Jones, 1987].

### 1.1.5 Alfvén waves

The Alfvén wave is named after Hannes Alfvén, who first theoretically predicted such waves in 1942 [Alfvén, 1942]. It is a low-frequency magnetohydrodynamic(MHD) wave propagating along the magnetic field, with perturbations of the perpendicular electric and magnetic fields. Assuming plasmas as a highly conducting, magnetized, and incompressible dynamic fluid, the ideal MHD theory results in three wave modes: fast, Alfvén, and slow modes. The dispersion relation of ideal Alfvén wave is $\omega = kv_A$, where $v_A = B_0/(\mu_0 n_i m_i)^{1/2}, B_0$ is the magnetic field strength, $\mu_0$ is the permeability of the plasma, $n_i$ is the ion number density, and $m_i$ is the ion mass.

Alfvén waves transport energy and momentum along the magnetic field line. The inertial Alfvén waves play essential roles in accelerating field-aligned electrons [Kletzing, 1994; Thompson and Lysak, 1996]. Particle acceleration in the polar cap boundary region is observed to be associated with propagating Alfvén waves [Chaston et al., 2000; Ergun et al., 2006]. Su et al. [2001] and Chaston et al. [2002a, b; 2003] have shown that the field-aligned counter-streaming electron bursts coincide with Alfvén waves.

In this thesis, we plan to establish a possible relationship between S-burst AKR and Alfvén waves in a dynamic Alfvénic acceleration region, i.e., polar cap boundary acceleration region.

## 1.2 Three auroral regions

### 1.2.1 The upward current region

The upward current region is an area containing upward field-aligned currents, convergent electric fields, and parallel potential drops as shown in the middle panel of Figure 1.1. In this region, the electric field vector points toward the center of the structure following equipotential contours. At the bottom of the structure, an arrow points upward,

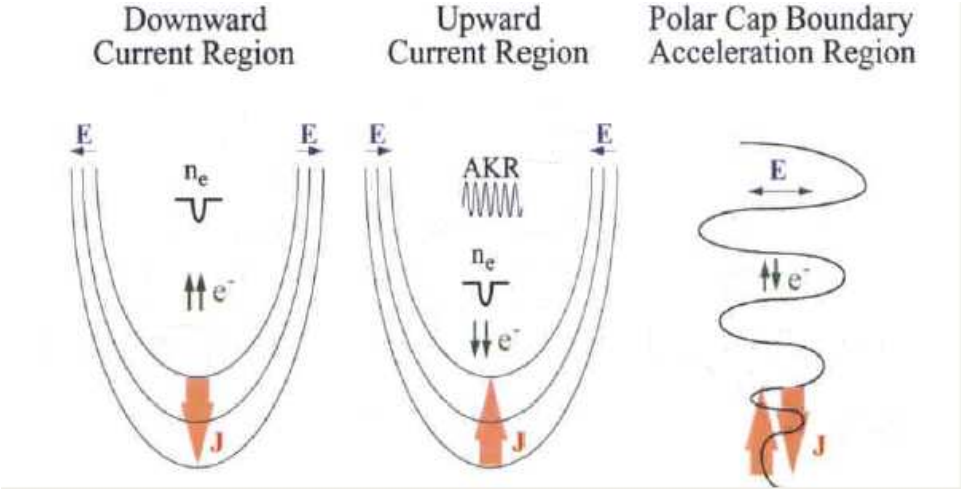


Figure 1.1. Illustration of a downward current region, an upward current region, and an Alfvénic acceleration region. Adapted from Carlson et al., 1998.

indicating an upward current carried by downward electrons. The prominent features of this region are up-going ions and down-going accelerated electrons, peaked in energy, with broad pitch angle distributions. The parallel potential drops have been demonstrated as a dominant source of auroral particle acceleration by FAST satellite observations [Carlson et al., 1998a]. In addition, large-amplitude ion cyclotron waves and electric field turbulences have also been observed in this region [Cattell et al., 1998; Carlson et al., 1998a].

Auroral density cavities are usually observed in the upward current region [Strangeway et al., 1998; Carlson et al., 1998a]. Evidence were shown that the FAST satellite passed directly through the cavity [e.g., Ergun et al, 2000b]. In the cavity, the dominant particles are accelerated down-going magnetospheric electrons and accelerated up-going ionospheric ions. The density cavity in the upward current region has been identified as the source region of AKR emissions [Ergun et al., 1998].

The "inverted-V" patterns in electron energy spectrograms [Frank and Ackerson, 1971] were often observed in the upward current region. The "U"-shaped potential struc-

ture was suggested to explain this phenomenon [Gurnett, 1972]. Electrons are accelerated along the magnetic field line by the parallel electric field. The acclerated electrons collide with the atmosphere to create visible aurora [Carlson et al., 1998a].

### 1.2.2 The downward current region

The downward current region contains downward field-aligned currents with divergent electric field structures as shown in the left panel of Figure 1.1. The up-going accelerated electrons and down-going accelerated ions are prominent features in this region. The curved potential structures have been indicated in the majority of downward current regions by Hwang et al. [2006 (a),(b)]. Based on FAST observations, the energies of up-going beams of field-aligned electrons are able to reach several keV [Carlson et al., 1998b]. They are the dominant features in the downward current region and presumably associated with the "black aurora", which is the optical counterpart of bright discrete arcs.

A parallel electric structure has been observed in the downward current region by the FAST satellite [Carlson et al., 1998a]. It can be described as a strong double layer. The direct measurement of the double layer indicates that this structure is dynamic and moving upward. The observation also supports the concept of multiple double layers [Andersson et al., 2002; Ergun et al., 2003]. Several double layers may combine to a large-scale potential structure; however, the detailed mechanism is a subject for future study.

Extremely low frequency electric field turbulences exist in downward current region, as well as the ion cyclotron waves [Carlson et al., 1998a]. Wave turbulence is often observed within the downward current region [Andersson et al, 2002; Ergun et al., 2003]. Density cavities can also be observed in this region, but usually their scales are smaller than those observed in the upward current region [Carlson et al., 1998a].

The downward current region is rarely associated with detectable auroral emissions. On the other hand, the upward current region has the most obvious signature – the visible aurora. The downward current region is more dynamic [Andersson et al., 2002], however, its properties have been less explored than those of the upward current region.

### 1.2.3 The polar cap boundary acceleration region

The polar cap boundary acceleration region is a unique auroral region near the open-closed magnetic field line boundaries where particle acceleration is dominated by waves rather than the quasi-static potential structures found in the upward and downward current regions. The low frequency electromagnetic waves observed by FAST are the low-altitude signatures of Alfvén waves observed by the POLAR spacecraft in the plasma sheet boundary layer [Wygant et al., 2000; Keiling et al., 2001, 2003].

The polar cap boundary acceleration region includes the dayside cusp and near midnight polar cap boundary, which map to the reconnection regions on the dayside magnetopause and the nightside magnetotail, respectively. The magnetic reconnection has been suggested to be an energy source of Alfvén waves [Wang et al., 2002]. In addition, the ratio of electric to magnetic field fluctuations in these regions is approximately equal to the local Alfvén speed, indicating the existence of Alfvén waves [e.g., Su et al., 2001]. Hence, the polar cap boundary acceleration region is also called the Alfvénic acceleration region. Alfvén waves were indicated as a substantial energy input during an active auroral event by Knudsen et al. [1990]. In addition to the electron flux accelerated by quasi-static electric fields along the magnetic field line, Keiling et al. [2003] suggested that the energy flows of high-altitude Alfvén waves contribute to both the dayside and nightside aurora emissions based on one-year Polar data.

A general method in identifying upward and downward current regions is by examining the slope of $\delta B_{\perp}$, the component of magnetic field perturbation perpendicular

to the spacecraft trajectory. Elphic et al. [2001] showed that a negative slope indicates an upward current, while a positive slope is a feature of a downward current region in the Northern Hemisphere. Moreover, inverted-V electrons and upward ion beams are usually observed in upward current regions, while up-going electrons and downward ions are often observed in downward current regions [Elphic et al., 2001].

Several distinct features in the polar cap boundary acceleration region are summarized here: (1) highly variable currents, which can be temporally or spatially average to little net current; (2) the frequency of strong wave power of several Hz; (3) the ratio of electric field and magnetic field perturbations ($\delta E/\delta B$) in the order of ($10^4 km/s$), similar to that of the local Alfvén speed; (4) counter-streaming field-aligned electron beams; and (5) enhanced energy fluxes of ion conics.

### 1.3 The FAST mission

The research work described in this thesis is based on data obtained from the Fast Auroral SnapshoT (FAST) satellite. The satellite was launched on August 21, 1996 with apogee of 4200 km altitude and perigee of 350 km altitude in an elliptical polar orbit ($83^0$ inclination). The spacecraft is still collecting data on its orbit. The FAST mission was developed to investigate the small scale structures in the aurora acceleration region at its relatively low altitude. Before the FAST mission, the basic features of the mid-altitude AAR had been discovered by a succession of satellites, such as S3-3, Viking, and Akebono. The FAST and Freja spacecraft were designed to study a large variety of small scale structures below and at the lower boundary of AAR [Lundin et al., 1994; Carlson et al., 1998a].

FAST traverses the low altitude auroral acceleration region providing high spatial and temporal resolution measurements of charged particles and electric and magnetic

fields. It crosses the auroral zones four times per orbit over a wide range of altitudes, local times, and seasons as its orbit motion evolves throughout the year.

FAST takes advantage of the fact that auroral processes occur only within limited latitudinal bands, typically 10-15 degrees wide circling the earth's magnetic poles. Thus, at low and medium magnetic latitudes the instruments on the satellite are switched off. Instruments are switched to a slow survey mode when the satellite crosses $60^0$ invariant latitude. The data rate increases by one order of magnitude higher in the fast survey mode, which is triggered by the enhancement of the auroral activity (e.g., enhanced electron energy flux). For the most intense events, the instruments are programmed to switch to the burst mode, taking high resolution "snapshot" measurements. In the burst mode, the data rate can reach 8 MB/s[Carlson et al., 1998a]. Typically, the burst data span 10-30 seconds and allow the detailed investigation of small-scale structures of AAR such as the fine structure of AKR recorded by Plasma Wave Tracker (PWT). Detailed descriptions can be found on the FAST web site at http://sprg.ssl.berkeley.edu/fast. In summary, the survey mode provides observations of large-scale features, while the burst mode obtains data with small-scale fine structures.

The data analysis in this thesis utilizes two software packages: Science Data Tool (SDT) and Interactive Data Language (IDL). SDT is a quick-look program for visual inspection purposes. The entire FAST data set is stored at the Space Science Laboratory (SSL) at the University of California at Berkeley (UCB). With the Data Manager (DM) program in conjunction with SDT, we are able to download FAST data files directly from SSL/UCB. For the last 10.5 years, the FAST team has developed subroutines written in IDL. Those subroutines were provided by the FAST team at UCB to the University of Texas (UT) at Arlington for data analysis purpose.

The method in searching for events of interest is described in Chapter 2. Seven new events of short burst AKR emissions are displayed in Chapter 3. We summarize the

properties of the S-bursts associated with Alfvén waves. Also, electron densities for 44 Alfvénic cases are estimated and the results are presented in Chapter 3.

# CHAPTER 2

# METHOD

## 2.1 Introduction

A possible relationship between S-burst AKR and Alfvén waves was suggested by Ergun et al. [2006]. The physical mechanism of energy transfer on Jupiter is suggested to be similar to that on Earth. By analyzing FAST satellite data, we are able to study Earth-based S-burst events and to explore a possible auroral acceleration mechanism suitable for both Earth and Jupiter. Since the magnetic field of Earth is relatively weak compared to that of Jupiter, we expect to obtain fewer Earth-based S-burst events based on the criterion of $\omega_{pe}/\omega_{ce} << 1$. Prior to the present, only one Earth-based S-burst event was reported by Ergun et al. [2006]. Su et al. [2007] presented simulation results to explain the key observed characteristics and indicated that a systematical search of S-burst radiation is needed.

The FAST satellite provides data from thousands of orbits every year. We examined data during the first three years of instrument operation (1997-1999). Data are plotted in various formats by utilizing SDT and FAST IDL subroutines. There are about ten thousand satellite orbits from three years. In order to manage searching a large amount of data, it is necessary to find an efficient method to seek the events of interest. In this thesis, an Alfvénic acceleration event is identified when Alfvén waves rather than quasi-static potential structures dominate particle accelerations, while S-burst AKR event is selected by the coexistence of Alfvén waves and S-burst emissions.

In this chapter, we first introduce observational characteristics of Alfvén waves and S-bursts. Next, we present the methods for determining the source region of AKRs. The

ability of event identification was gradually established based on our experiences, which are presented in the last section of Chapter 2.

## 2.2 Observational characteristics of Alfvénic acceleration event

An Alfvénic acceleration event is associated with particular characteristics in particle and field data. For example, enhanced electron fluxes associated with Alfvén waves are different from "inverted-V" electrons accelerated by quasi-steady parallel electric fields. An example is shown in Figure 2.1. Three observational signatures of an Alfvénic acceleration event are described here:

(1)The fluctuations of magnetic fields (Figure 2.1a) and electric fields (Figure 2.1b) indicate the existence of Alfvén waves. In observational field data, it is difficult to separate low frequency Alfvénic perturbations from the static current structure. By using impedance function $Z(f) = \mu_0 \mid \delta E(f)/\delta B(f) \mid$, Knudsen et al. [1990] showed a distinction between quasi-static structure and Alfvénic fluctuations at a frequency  0.1 Hz. In our study, we select 0.2 Hz as our lower frequency boundary to avoid quasi-static contribution. Observed electric fields are filtered to exclude the static current contribution ($< 0.2$Hz) and higher frequency waves (>10 Hz, local $O^+$ cyclotron frequency) to isolate Alfvénic fluctuations.

(2)The ratio of electric field fluctuations to magnetic field fluctuations ( $\delta E/\delta B$) is in the same order of magnitude of the local Alfvén speed (on the order of $10^4$ km/s) [Chaston et al., 1999; Su et al. 2001].

(3)The quasi-static electric field is able to accelerate electrons forming an "inverted-V" pattern in energy spectrograms [Gurnett, 1972]. In the polar cap boundary region, inertial Alfvén waves dominate the electron acceleration in the field-aligned direction and the electron fluxes entend over a broad energy range [Ergun et al.,2005]. In contrast with the classical "inverted-V" signatures (1997-01-07/12:13:50 to 1997-01-07/12:14:33 UT in

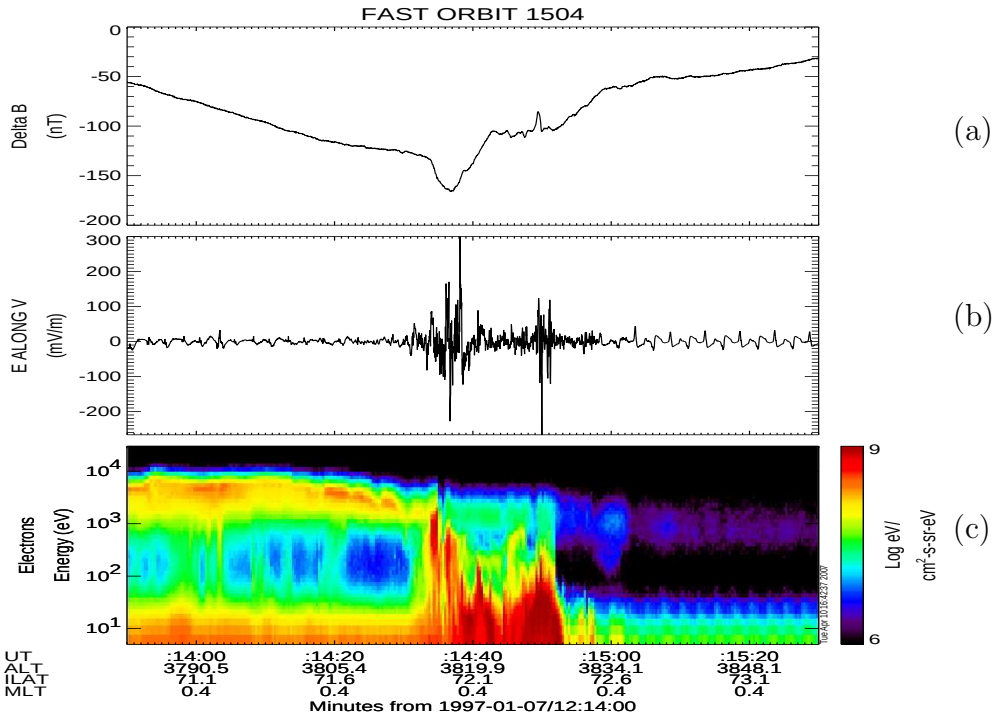


Figure 2.1. An example of Alfvénic acceleration event. (a) The magnetic field perturbation in the direction perpendicular to the satellite trajectory. (b) The electric field along the satellite trajectory. (c) The electron energy spectrogram. The Alfvénic acceleration region is from 12:14:43 to 12:14:53 UT on 1997-01-07, while "inverted-V" electrons are seen from 12:13:50 to 12:14:33 UT.

Figure 2.1c), the Alfvénic accelerated electrons are broad and continuous in energy. An example can be seen from 12:14:43 to 12:14:53 UT on 1997-01-07.

## 2.3 The differences between S-bursts and AKRs

In general, AKR emissions can be analyzed in both the burst and survey modes of Swept Frequency Analyzer (SFA). For fine structure measurements such as S-bursts, the high-resolution data were obtained from Plasma Wave Tracker (PWT). A plot of electric field spectral power density is shown in Figure 2.2, where the discrete short bursts were present. In contrast, a typical AKR emission such as that shown in Figure 2.3 has no distinct discreteness.

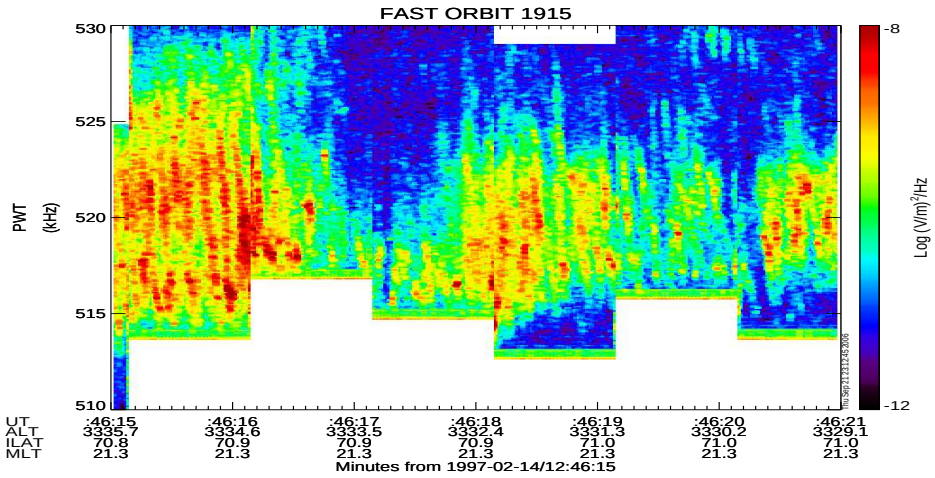


Figure 2.2. Short-burst emissions obtained from Plasma Wave Tracker (PWT). Discrete emission pulses reoccur during 12:46:15-21 UT on 1997-02-14 .

## 2.4 The source region of AKR emissions

The source region of emissions can be calculated approximately from the following procedures. A dipole magnetic field is assumed to simplify our calculation, $B = \mu_0 m(2\cos\theta\hat{r} + \sin\theta\hat{\theta})/4\pi r^3$ in the spherical coordinate system. Hence,

$$B \propto 1/r^3 \tag{2.1}$$

where $r$ is in the unit of geocentric distance ($R_E$).

$$B_A/B_s = (r_s/r_A)^3 \tag{2.2}$$

where $r_A$ represents the source region of emissions, while $r_s$ represents the satellite location. $B_A$ and $B_s$ represent the magnetic field at the source region and at the satellite location, respectively. The local electron cyclotron frequency is

$$\omega = eB/m_e \tag{2.3}$$

where $B$ is the local magnetic field, $e$ and $m_e$ are the electron charge and electron mass, respectively.

$$\omega_A/\omega_s = B_A/B_s = (r_s/r_A)^3 \tag{2.4}$$

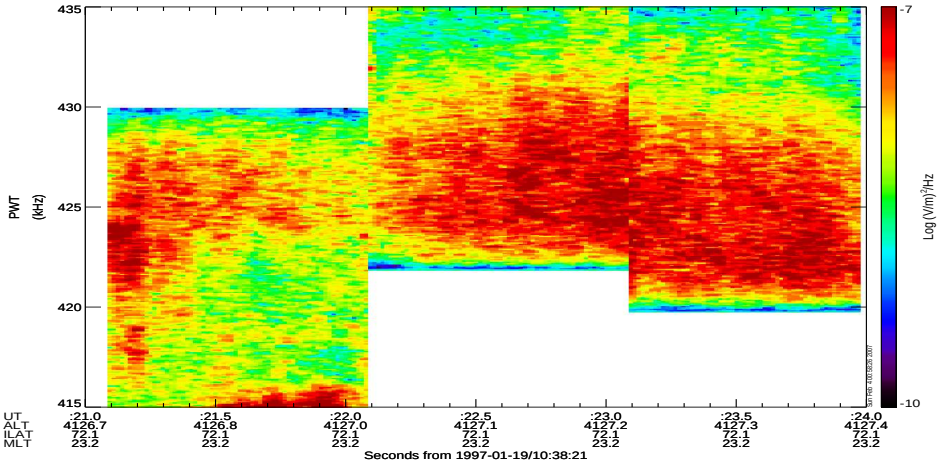


Figure 2.3. AKR emissions obtained from PWT. No discrete emission pulses were seen.

The source region of the emission is estimated by the following equation.

$$r_A = r_s(\omega_s/\omega_A)^{1/3} \tag{2.5}$$

where the local electron cyclotron frequency at the location of satellite ($\omega_s$) is obtained from equation 2.3, $\omega_A$ is the emission frequency obtained from PWT, and $r_s$ is the geocentric distance of the satellite.

## 2.5 Processes in identifying S-burst AKR emissions

The processes in identifying the events of interest evolved gradually from our experience. We generalized the processes into four stages. More restrictions were included in later stages to speed up the screening process. It should be noted here that although the restrictions enhanced the efficiency of the scanning, some possible events may have been excluded. In addition to the case reported in Ergun et al. [2006] and Su et al. [2007], seven S-burst events were found.

### 2.5.1 The first stage - identifying S-burst during substorms

Our screening process started with the FAST data obtained on 01/01/1997, orbit number 1436. Originally, high-resolution data were checked for every orbit, which was very time consuming. Ergun et al. [2006] showed that S-bursts are observed during the recovery phase of the substorm. In general, substorms are associated with high Auroral Electrojet (AE) indices. Hence, we screened FAST data when AE indices were higher than 150. The information of AE was obtained through the website provided by the World Data Center for Geomagnetism in Kyoto [http://swdcwww.kugi.kyoto-u.ac.jp/aedir/]. It should be noted that we also checked data during non-substorm periods occasionally throughout the entire process, the Alfvénic acceleration event occurs infrequently during those periods.

Enhanced counter-streaming electrons are associated with Alfvénic perturbations [Su et al., 2001; Chaston et al., 2002a, b; Lysak and Song, 2003]. Hence, we utilize these distinct characteristics to identify possible candidates through summary plots on the official FAST website provided by UC Berkeley.

During the screening process for possible Alfvénic acceleration events, six types of detail plots were examined: (1) the magnetic field perturbations perpendicular to the spacecraft trajectory; (2) the electric field along the satellite trajectory; (3) the electron energy spectrogram; (4) the electric field spectral power density obtained by SFA in the survey mode; (5) the electric field spectral power density in the burst mode; and (6) the local electron cyclotron frequency. An example is shown in Figure 2.4. The first three panels help us to identify the Alfvénic acceleration region, while Panels (4) and (5) capture AKR emissions if present. The local electron cyclotron frequency ($\omega_s$) in panel (6) is estimated from the total magnetic field obtained from the instrument. It is used to estimate the location of emission source as described in Section 2.4.

When AKR emissions, enhanced counter-streaming electrons, and Alfvénic perturbations were observed simultaneously, high-resolution data from PWT were selected for further examination of fine structures.

The above method was applied to 2290 orbits (orbits 1436-3726) from January 1 to August 1, 2007. 186 orbits were identified manually where the enhanced electron fluxes were associated with Alfvénic perturbations. In summary, the minimum occurrence rate of Alfvénic acceleration events is estimated to be 8%. Additionally, three events were identified where short-burst AKR signatures exist simultaneously with Alfvénic accelerated electrons: (1) orbit 1504 at 12:14:49 - 52 UT on 01/07/1997; (2) orbit 1589 at 08:56:48 - 51 UT on 01/15/1997; and (3) orbit 1915 at 12:46:15 - 19 UT on 02/14/1997.

### 2.5.2 The second stage - identifying S-burst by intensity restrictions

More than half of the data in 3 years were examined under the criteria of AE $> 150$ as described above. The method in the first stage is not efficient. We found that many Alfvénic events do not associated with visible emission signals recorded by SFA or PWT. Moreover, the electron fluxes of AKR events were higher than those of non-AKR events. As a result, we focused on the Alfvénic events with the following three characteristics: (1) The energy of field-aligned electrons exceeds 100 eV; (2) The corresponding electron energy flux is higher than $10^9\ eV/(cm^2 - s - sr - ev)$; and (3) The event should last at least $\sim$ 1 minute.

The SDT quick look software is very helpful as a screening tool. An example of AKR emissions associated with enhanced electron fluxes is shown in Figure 2.5.

The Data Manager (DM) program is designed to communicate with the FAST data center in UC Berkeley. The users may download FAST data directly through the Berkeley server. We found that if the data size is less than 60 MB per orbit, it is not

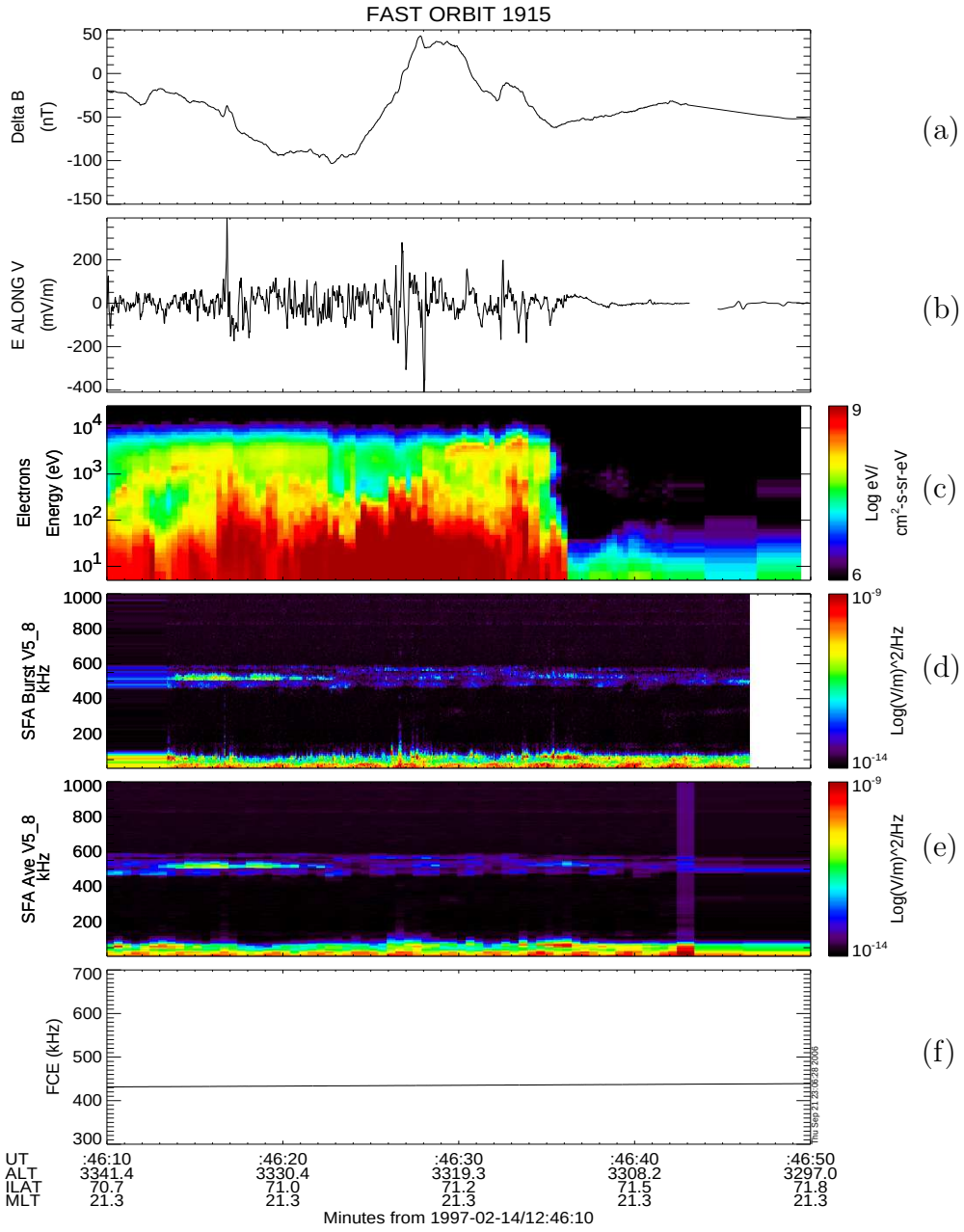


Figure 2.4. An example of short-burst emissions observed by the FAST satellite. (a)The magnetic field perturbations in the direction perpendicular to the satellite trajectory. (b) The electric field along the satellite trajectory. (c) The electron energy spectrogram. (d) The electric field spectral density in the burst mode. (e)The electric field spectral density in the survey mode. (f) The local electron cyclotron frequency.

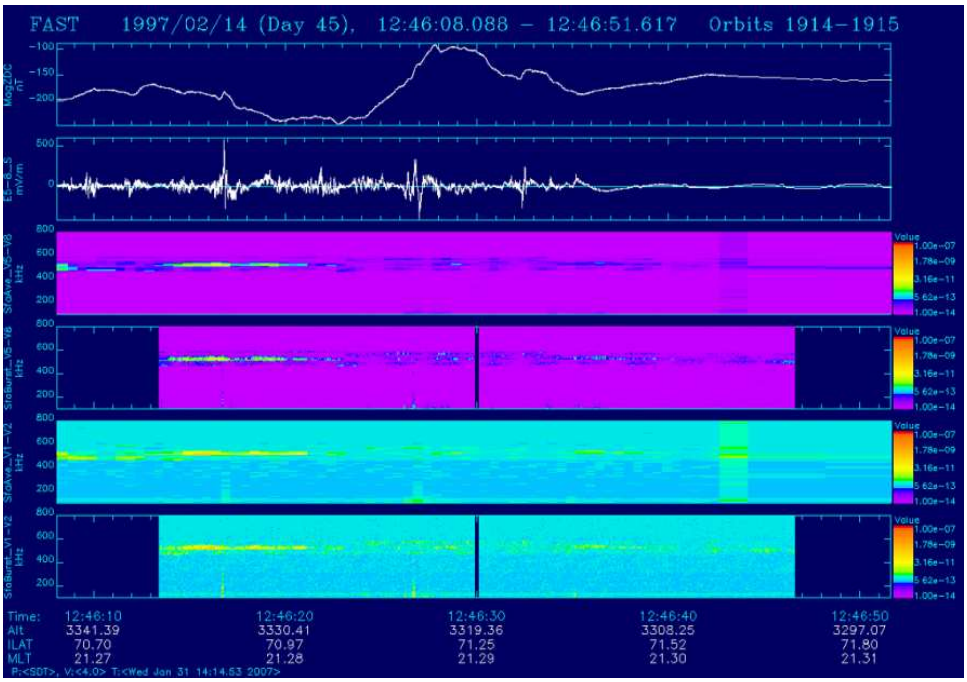


Figure 2.5. An example of AKR emissions associated with enhanced electron fluxes of orbit 1915, from 12:46:15 to 12:46:21 UT on 1997-02-14. The perturbations of magnetic and electric fields are shown in the first and second panels. The survey and burst modes of the power density obtained from Probe V1-V2 of SFA are plotted in the third and fourth panels, while data from Probe V5-V8 of SFA are displayed in the fifth and sixth panels .

sufficient to include AKR signals. Hence, we eliminated data with size less than 60 MB in order to increase the efficiency of the screening process.

The method described above was applied to data from 08/01/1997 to 06/05/1998 (orbits 3727-7067). Based on the criteria described in this subsection, one S-burst AKR event (orbit 6903) was found during 01:08:31-38 UT on 05/21/1998.

### 2.5.3 The third stage - identifying S-burst by anisotropic fluxes

The common feature of four events reported in subsections 2.5.1-2.5.2 is that the electron energy flux in the parallel direction (along the magnetic field line) is one or two orders of magnitude higher than that in the perpendicular direction. The electron

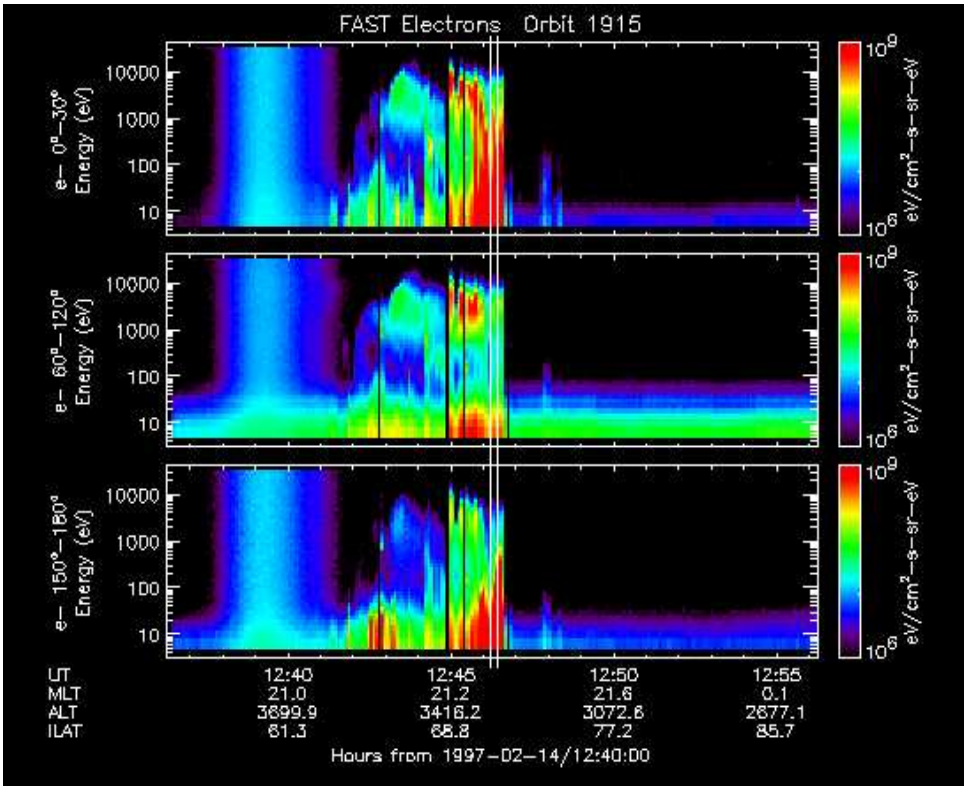


Figure 2.6. Electron energy spectrograms in various pitch angles for orbit 1915, from 12:40 to 12:55 UT on 1997-02-14: (a) $0^0 - 30^0$ , (b) $60^0 - 120^0$ , and (c) $150^0 - 180^0$ . The interval between two white vertical lines is where S-burst AKR coexist with the enhanced field-aligned electrons..

energy spectrograms with various pitch angles are shown in Figure 2.6, where pitch angles $0^0 - 30^0$, $60^0 - 120^0$ and $150^0 - 180^0$ are plotted in the top, middle, and bottom panels, respectively. It should be noted that $0^0$ is the direction along the field line (downward in the Northern hemisphere), while $180^0$ is the upward direction.

With the criterion of the anisotropic signatures of electrons, we reexamined the 186 Alfvénic cases reported in section 2.5.1, as well as data from 08/01/1997 to 08/06/1998. We found 41 Alfvénic events with the ratio of $F_\perp$ / $F_\parallel \leq 0.1$ (i.e., $F_\perp$ is at least one order of magnitude smaller than $F_\parallel$), where $F_\perp$ and $F_\parallel$ represent peaks of the perpendicular ($60^0 - 120^0$) and parallel ($0^0 - 30^0$ or $150^0 - 180^0$) electron flux, respectively.

Those 41 cases were selected for further examination in searching for short burst emissions. We identified the same four events reported in subsection 2.5.1 and 2.5.2. No additional event was found between August 1 1997 and August 6 1998.

### 2.5.4 The fourth stage - identifying S-burst at the nightside and at high altitudes

The Alfvénic acceleration events with prominently parallel electron flux anisotropy are only found at the nightside. We therefore restricted our search at the nightside for the remaining data between 08/06/1998 and 12/31/1999. Moreover, the strongly field-aligned electron flux anisotropy $F_{\perp}/F_{\parallel} \leq 0.1$ is infrequently observed at altitudes $< 2500$ km at night. Thus, we eliminated orbits which were below 2500 km altitudes to speed up the screening process.

With all constraints described in subsections 2.5.1-2.5.4, we reexamined the entire 3-year dataset. Three additional events were discovered: (1) orbit 1845 at 01:17:06-11 UT on 02/08/1997, (2) orbit 1940 at 20:13:45-50 UT on 02/16/1997, and (3) orbit 1952 at 22:49:49-54 on 02/17/1997.

# CHAPTER 3

# RESULTS

## 3.1 Introduction

Based on the methods described in the previous section, eight cases were identified where the short-burst emissions were simultaneously observed with Alfvénic acceleration signatures including the one (orbit 1906) previously reported by Ergun et al. [2006]. The characteristics of such events are discussed in Section 3.2, while unstable electron distributions associated with short-bursts are presented in Section 3.3. Finally, the density anisotropy at the nightside is compared with that in the dayside in Section 3.4.

## 3.2 Characteristics of S-burst AKR events

Eight S-burst AKR events are listed in Table 3.1. The characteristics of these short burst emissions (Figure 3.1-3.8) are discussed below:

(1) All of them occurred at the nightside, particularly between 21:00 and 1:00 magnetic local time (MLT). Relatively low ionization and plasma density are expected at the nightside, while a higher density is anticipated in the dayside due to a higher ionization rate. Hence, the plasma environment at the nightside is more likely to meet the low density criterion (i.e., $\omega_{pe}/\omega_{ce} << 1$) than that of the dayside. A low plasma density is necessary to provide a small plasma frequency and to satisfy the condition for the electron cyclotron maser or the upper hybrid wave conversion to generate AKR emissions.

(2) All of the identified events occurred during winter. Two of them were observed in January and five in February. The majority of events were obtained in the Northern

Hemisphere, while one event (orbit 6903) observed in the Southern Hemisphere in May, 1998. The plasma density is lower in winter due to low ionization rates. Since one of the conditions for generating AKR is the low plasma frequency (i.e., low plasma density), this may be why the majority events were observed in winter months. Kumamoto and Oya [1998] found that AKR is more common in the winter hemisphere than in the summer hemisphere based on a seven-year survey of the occurrence and intensity of AKR.

Table 3.1. A list of the characteristics of eight S-burst AKR events

| Orbit | Date/MLT | Frequency Range (kHz) | Reoccurrence Rate (Hz) | Power Density $(v/m)^2/Hz$ | Satellite Altitude (km) | Source Location (km) | Distance (km)Below Satellite |
|---|---|---|---|---|---|---|---|
| 1504 | 01-07-97/0.4 | 475 - 482 | 7 - 9 | $10^{-8}$ | 3827 | 2930 - 2980 | 850 - 890 |
| 1589 | 01-15-97/23.8 | 437 - 452 | 8 - 10 | $10^{-7}$ | 4020 | 3200 - 3520 | 780 - 820 |
| 1845 | 02-08-97/22.9 | 457 - 466 | 10 - 17 | $10^{-8}$ | 3914 | 2980 - 3040 | 880 - 940 |
| 1906 | 02-13-97/22.8 | 558 - 568 | 10 - 18 | $10^{-8}$ | 3217 | 2760 - 2810 | 410 - 460 |
| 1915 | 02-14-97/21.3 | 515 - 525 | 8 - 10 | $10^{-8}$ | 3334 | 2710 - 2770 | 570 - 630 |
| 1940 | 02-16-97/22.7 | 465 - 470 | 8 - 10 | $10^{-7.5}$ | 3350 | 2920 - 2950 | 400 - 430 |
| 1952 | 02-17-97/22.3 | 500 - 510 | 8 - 10 | $10^{-8}$ | 3431 | 2670 - 2730 | 700 - 760 |
| 6903 | 05-21-98/0.8 | 398 - 406 | 9 - 10 | $10^{-7}$ | 4143 | 3540 - 3610 | 540 - 600 |

(3) In the plots of the electric field power spectral density obtained from the high-resolution PWT instrument, each burst presents a characteristic of a negative frequency drift as shown in the bottom panel of each case from Figures 3.1 to 3.8. This phenomenon indicates that the source location increases with decreasing local electron cyclotron frequency. In summary, the frequencies of S-bursts lie within a range of 398-568 kHz as listed in the third column of Table 3.1.

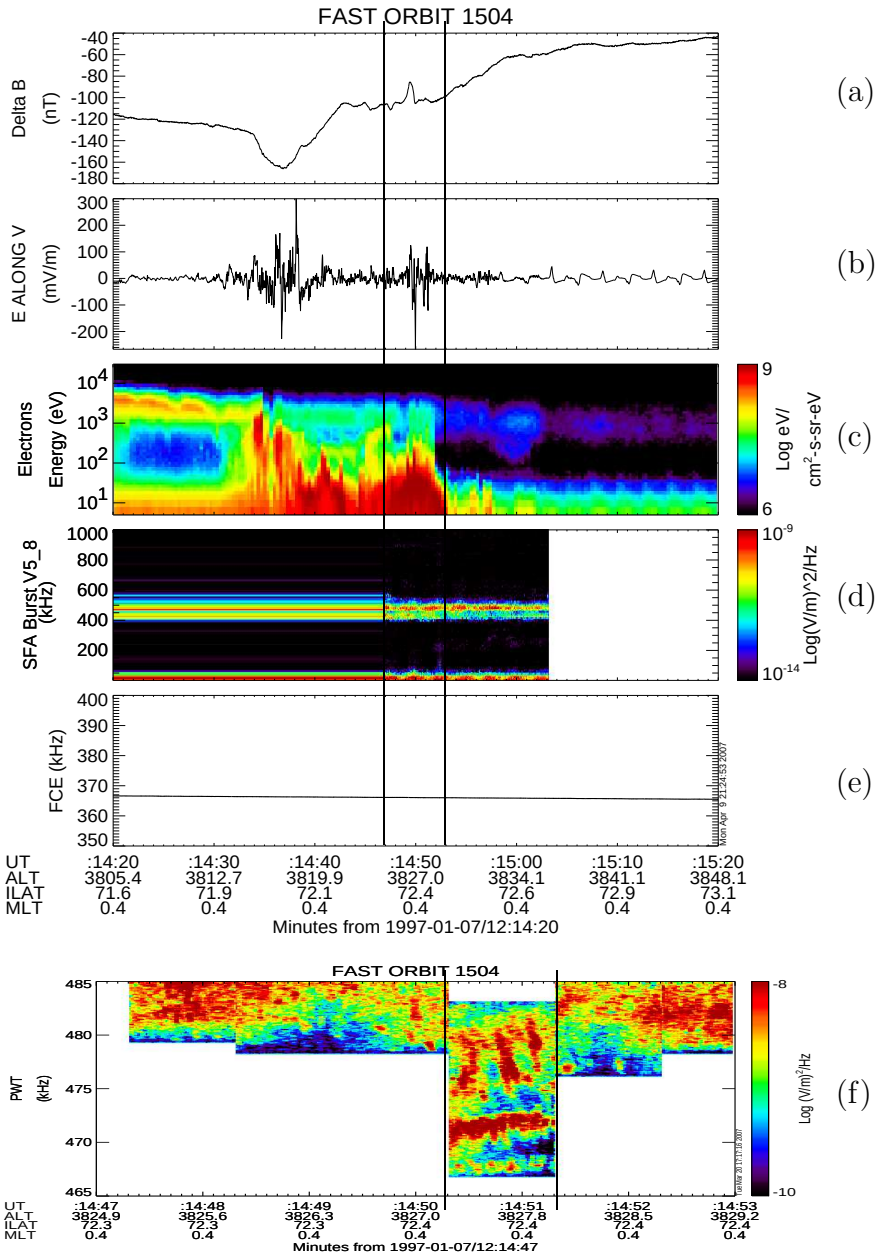


Figure 3.1. The S-burst AKR event of Orbit 1504, from 12:14:47 to 12:14:53 UT on 1997-01-07, associated with Alfvénic acceleration signatures. (a) The magnetic field perturbation in the direction perpendicular to the satellite trajectory. (b) The electric field along the spacecraft trajectory. (c) The electron energy spectrogram. (d) The electric field spectral power density obtained from SFA. (e) The local electron cyclotron frequency. (f) An expanded view of the electric field spectral power density from PWT at 12:14:47-53 UT. The vertical lines in panel (a)-(e) indicate the time period of interest. While S-burst emissions are shown between the two vertical lines in panel (f).

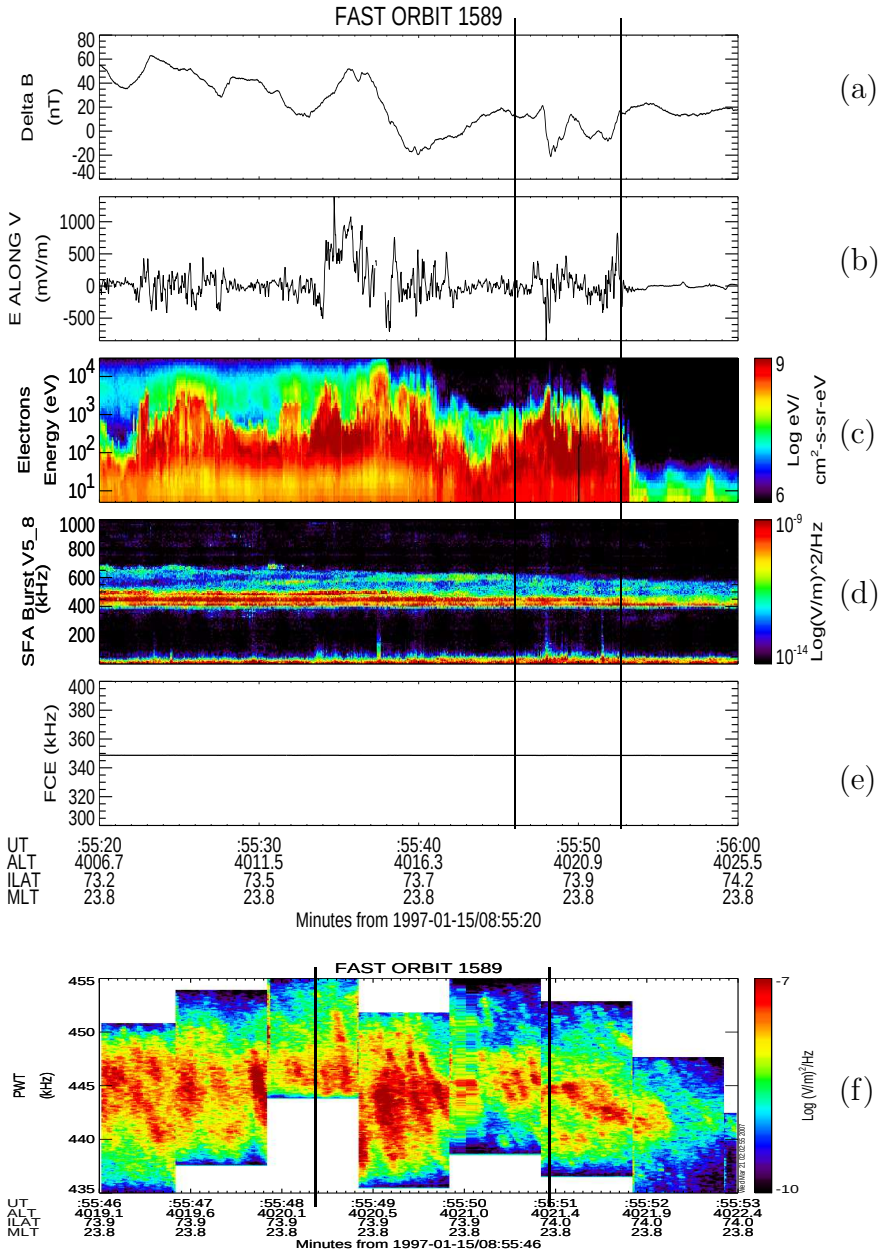


Figure 3.2. The S-burst AKR event of Orbit 1589, from 08:55:46 to 08:55:53 UT on 1997-01-15, associated with Alfvénic acceleration signatures. (a) The magnetic field perturbation in the direction perpendicular to the satellite trajectory. (b) The electric field along the spacecraft trajectory. (c) The electron energy spectrogram. (d) The electric field spectral power density obtained from SFA. (e) The local electron cyclotron frequency. (f) An expanded view of the electric field spectral power density from PWT at 08:55:46-53 UT. The vertical lines in panel (a)-(e) indicate the time period of interest. While S-burst emissions are shown between the two vertical lines in panel (f).

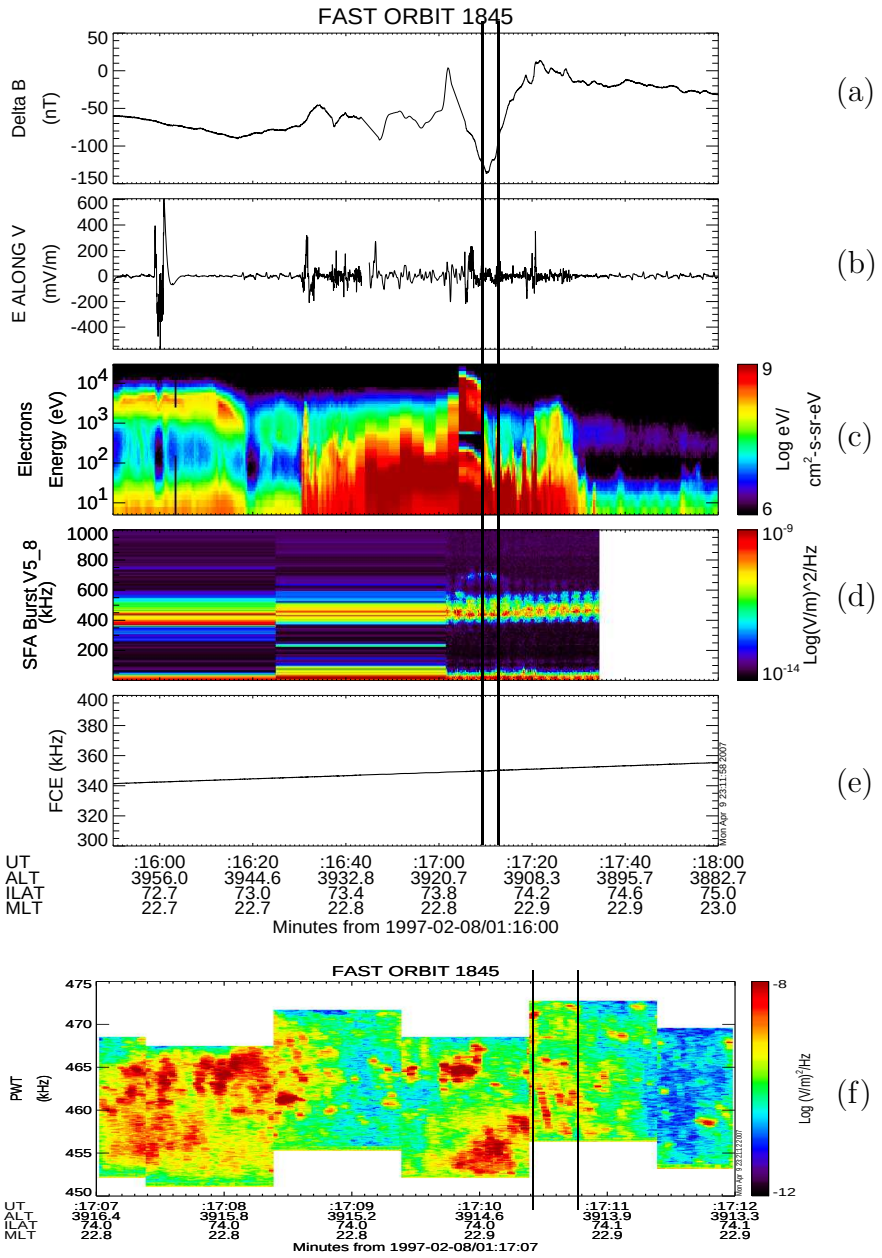


Figure 3.3. The S-burst AKR event of Orbit 1845, from 01:17:07 to 01:17:12 UT on 1997-02-08, associated with Alfvénic acceleration signatures. (a) The magnetic field perturbation in the direction perpendicular to the satellite trajectory. (b) The electric field along the spacecraft trajectory. (c) The electron energy spectrogram. (d) The electric field spectral power density obtained from SFA. (e) The local electron cyclotron frequency. (f) An expanded view of the electric field spectral power density from PWT at 01:17:07-12 UT. The vertical lines in panel (a)-(e) indicate the time period of interest. While S-burst emissions are shown between the two vertical lines in panel (f) .

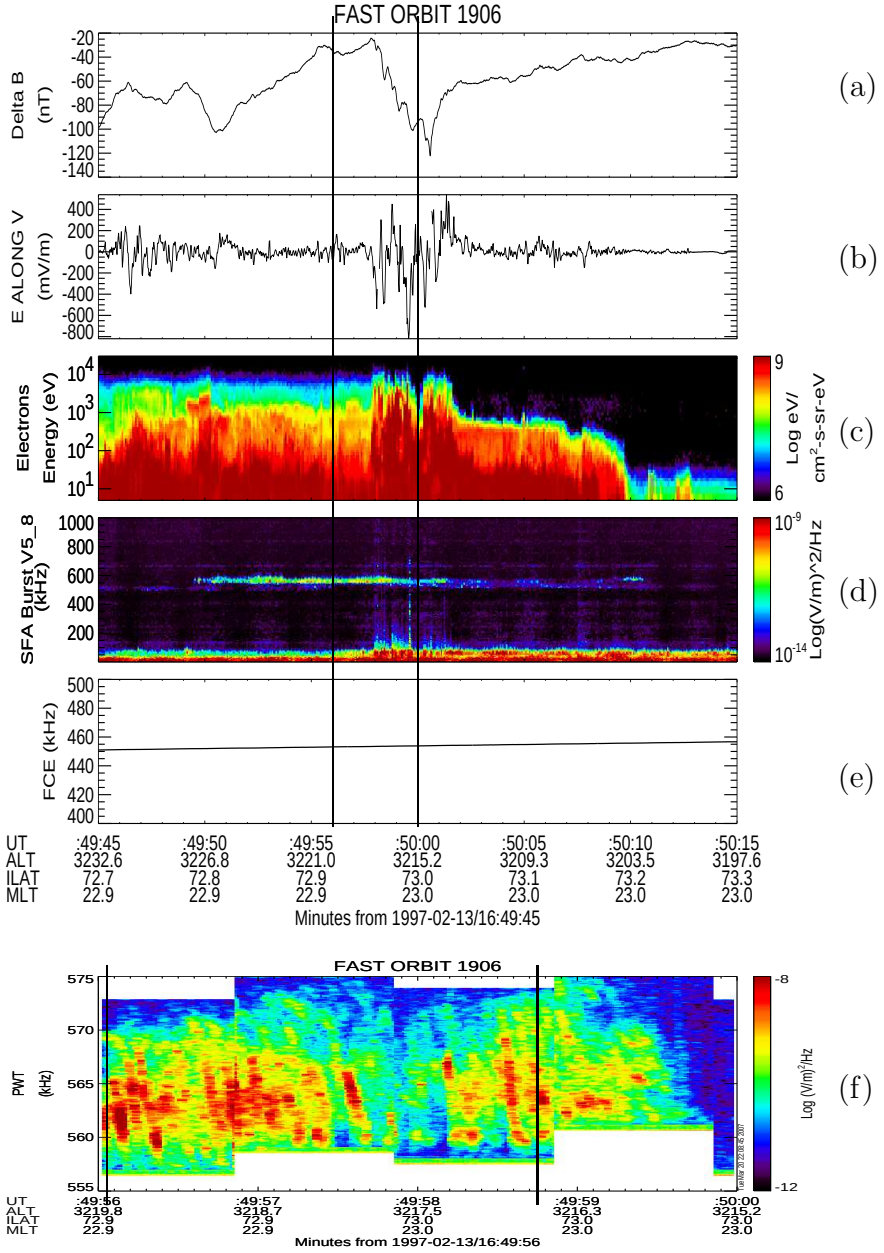


Figure 3.4. The S-burst event AKR of Orbit 1906, from 16:49:56 to 16:50:00 UT on 1997-02-13, associated with Alfvénic acceleration signatures. (a) The magnetic field perturbation in the direction perpendicular to the satellite trajectory. (b) The electric field along the spacecraft trajectory. (c) The electron energy spectrogram. (d) The electric field spectral power density obtained from SFA. (e) The local electron cyclotron frequency. (f) An expanded view of the electric field spectral power density from PWT at 16:49:56-50:00 UT. The vertical lines in panel (a)-(e) indicate the time period of interest. While S-burst emissions are shown between the two vertical lines in panel (f) .

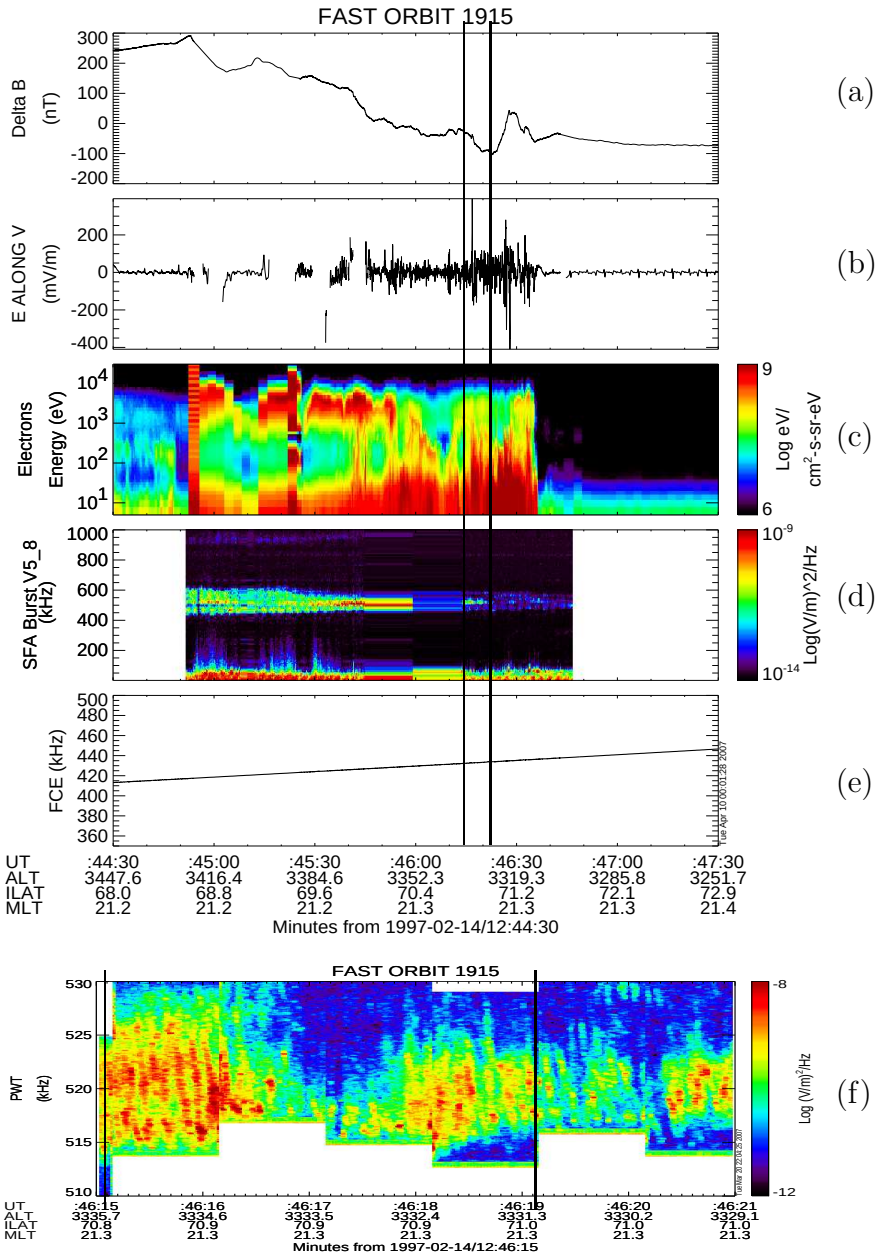


Figure 3.5. The S-burst event AKR of Orbit 1915, from 12:46:15 to 12:46:21 UT on 1997-02-14, associated with Alfvénic acceleration signatures. (a) The magnetic field perturbation in the direction perpendicular to the satellite trajectory. (b) The electric field along the spacecraft trajectory. (c) The electron energy spectrogram. (d) The electric field spectral power density obtained from SFA. (e) The local electron cyclotron frequency. (f) An expanded view of the electric field spectral power density from PWT at 12:46:15-21 UT. The vertical lines in panel (a)-(e) indicate the time period of interest. While S-burst emissions are shown between the two vertical lines in panel (f).

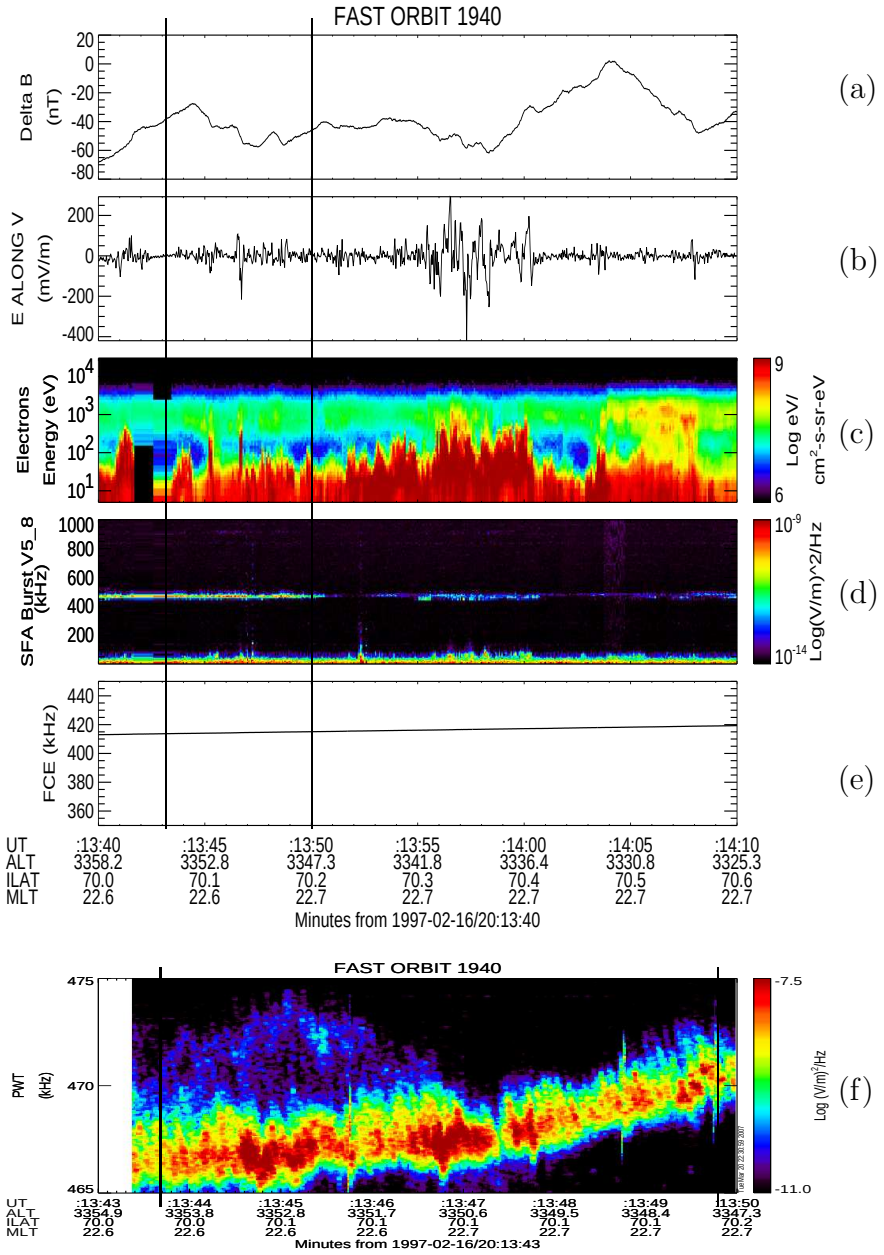


Figure 3.6. The S-burst event AKR of Orbit 1940, from 20:13:43 to 20:13:50 UT on 1997-02-16, associated with Alfvénic acceleration signatures. (a) The magnetic field perturbation in the direction perpendicular to the satellite trajectory. (b) The electric field along the spacecraft trajectory. (c) The electron energy spectrogram. (d) The electric field spectral power density obtained from SFA. (e) The local electron cyclotron frequency. (f) An expanded view of the electric field spectral power density from PWT at 20:13:43-50 UT. The vertical lines in panel (a)-(e) indicate the time period of interest. While S-burst emissions are shown between the two vertical lines in panel (f).

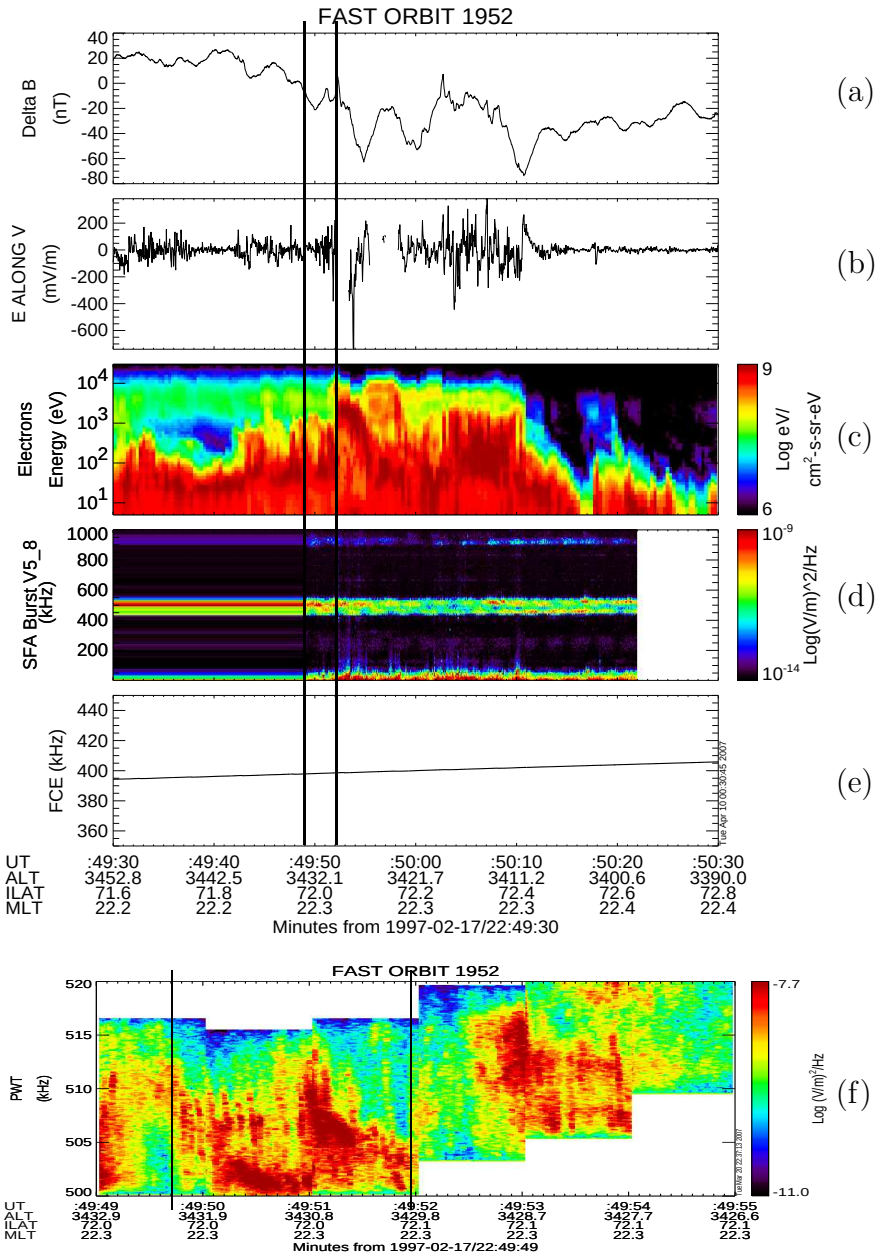


Figure 3.7. The S-burst event AKR of Orbit 1952, from 22:49:49 to 22:49:55 UT on 1997-02-17, associated with Alfvénic acceleration signatures. (a) The magnetic field perturbation in the direction perpendicular to the satellite trajectory. (b) The electric field along the spacecraft trajectory. (c) The electron energy spectrogram. (d) The electric field spectral power density obtained from SFA. (e) The local electron cyclotron frequency. (f) An expanded view of the electric field spectral power density from PWT at 22:49:49-55 UT. The vertical lines in panel (a)-(e) indicate the time period of interest. While S-burst emissions are shown between the two vertical lines in panel (f).

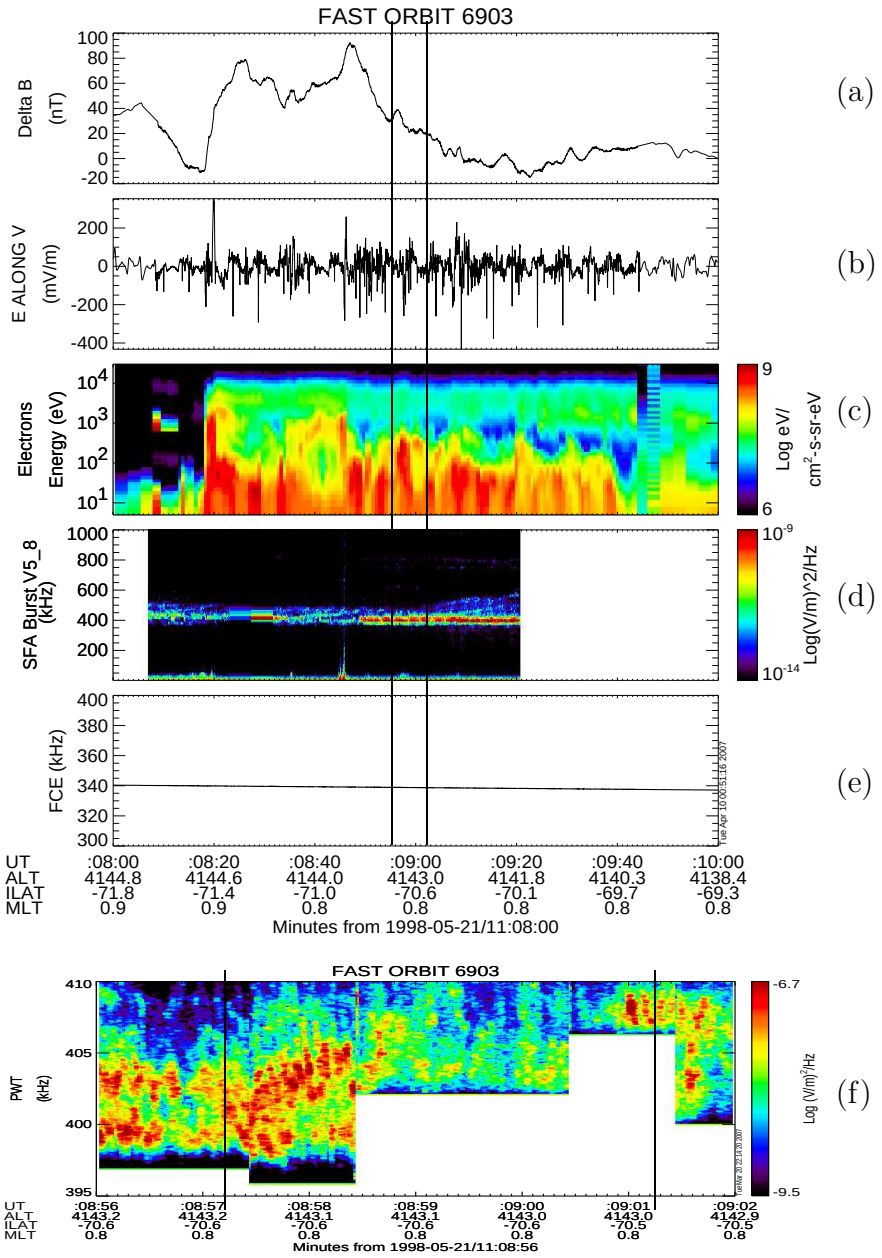


Figure 3.8. The S-burst event AKR of Orbit 6903, from 11:08:56 to 11:09:02 UT on 1998-05-21, associated with Alfvénic acceleration signatures. (a) The magnetic field perturbation in the direction perpendicular to the satellite trajectory. (b) The electric field along the spacecraft trajectory. (c) The electron energy spectrogram. (d) The electric field spectral power density obtained from SFA. (e) The local electron cyclotron frequency. (f) An expanded view of the electric field spectral power density from PWT at 11:08:56-09:02 UT. The vertical lines in panel (a)-(e) indicate the time period of interest. While S-burst emissions are shown between the two vertical lines in panel (f).

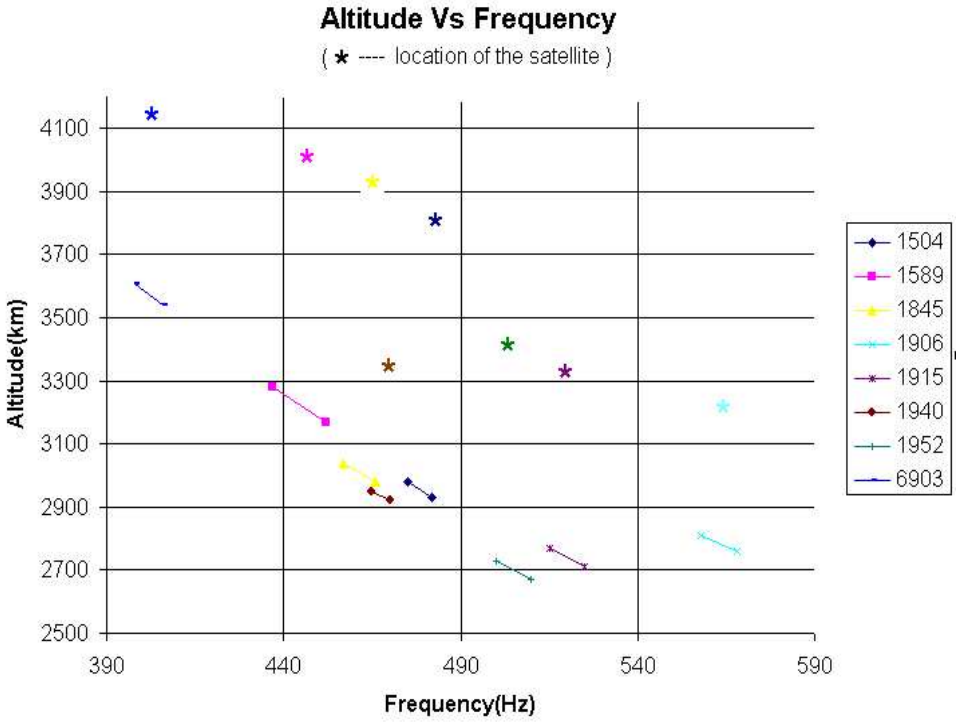


Figure 3.9. The source location of short bursts versus observed frequencies.

(4) The duration of a single burst is about 0.1 second. The location of AKR source region can be estimated by Eq. 2.5. From Table 3.1, the largest spatial scale of each burst is estimated to be $\sim$ 60 km. It should be noted that some bursts are difficult to distinguish manually. We counted the number of discrete pulses during a certain time interval to estimate the reoccurrence rate as those shown in the fourth column in Table 3.1. For all eight events, the reoccurrence rate is ranged between 7 and 18 Hz.

(5) The spectral power density of common AKR emissions observed from the FAST satellite is on the order of $10^{-6}(V/m)^2/Hz$. The spectral power density of S-burst emissions is one or two orders weaker than that of common AKRs. If S-bursts and AKRs are present simultaneously, it would be difficult to distinguish weak S-bursts from strong AKR signals. For events presented in Table 3.1, S-bursts did not overlap with AKR sig-

nals. The "inverted-V" electrons are known as a signature in the upward current region. Based on our results, no "inverted-V" signature was observed during S-burst periods.

(6) The source regions of short-burst emissions are typically located between 2600 and 3610 km above the Earth's surface. No event was obtained at low altitudes near the perigee altitude (∼315 km) of the satellite. In general, the plasma density decreases with increasing altitudes. Therefore, the low plasma density at mid-altitudes or high altitudes (relative to the FAST orbit) may be easier to meet the criterion of $\omega_{pe}/\omega_{ce} << 1$ in order to generate emissions.

A plot of the source location versus the short-burst frequency for eight events is shown in Figure 3.9. The emission is assumed to be generated from locally unstable electron distributions, hence, the emission frequency represents the local cyclotron frequency. The figure displays a negative slop which agrees with a converging magnetic field. In figure 3.9, the fluctuations departed from a negative line are due to various latitudes of AKR source regions and/or due to the dynamics of Earth's magnetic field.

(7) The emission source regions are below the satellite. The shortest distance between the source region and the satellite is about 400 km. Although we did not find cases in which S-bursts occurred above the satellite, this does not exclude the possibility that the AKR may occur above the satellite.

### 3.3 Electron flux Distributions

Su et al. [2007] suggested that short-burst emissions are generated from unstable electron distributions such as single and multiple shell distributions, as well as electron conic distributions. Electron distributions with 79 ms resolution were examined throughout the time intervals when short-burst emissions were present. The results are summarized in Table 3.2.

Table 3.2. Different types of electron energy flux distributions

| orbits | Distribution types |
|---|---|
| 1504 | Single shell and Conic distributions |
| 1589 | Single shell, Double shell and Conic distributions |
| 1845 | Loss-cone and Single shell distributions |
| 1906 | Single, Double, Triple shell and Conic distributions |
| 1915 | Single shell and Conic distributions |
| 1940 | Single shell, Double shell and Conic distributions |
| 1952 | Single, Double, Triple shell and Conic distributions |
| 6903 | Single shell, Double shell and Conic distributions |

Examples of various electron flux distributions as function of electron parallel and perpendicular velocity from orbit 1589 and 1952 are plotted in Figure 3.10, where single-shell, double-shell, conic distributions are from orbit 1589 and shown in panels (a)-(c), triple-shell and loss-cone distributions are from orbit 1952 and shown in panels (d) and (e), respectively.

Single shell distributions existed in all events, while multiple shell distributions appeared in more than half of them. Su et al. [2007] suggested that the observed short bursts are generated from unstable electron distributions due to multiple Alfvénic perturbations, hence, parallel electric fields associated with inertial Alfvén waves are considered as a candidate to generate multiple shell distributions.

Conic distributions were observed in seven of the events. This type of distribution was called a "ring" distribution in Ergun et al [2006]. The "conics" are due to the magnetic mirror effect. Down-going electrons with large pitch angles ( $>$ loss cone) reflect back up the flux tube at the mirror point and form the conic distribution. This distribution is also considered to be a candidate to generate electron maser instability by Su et al. [2007].

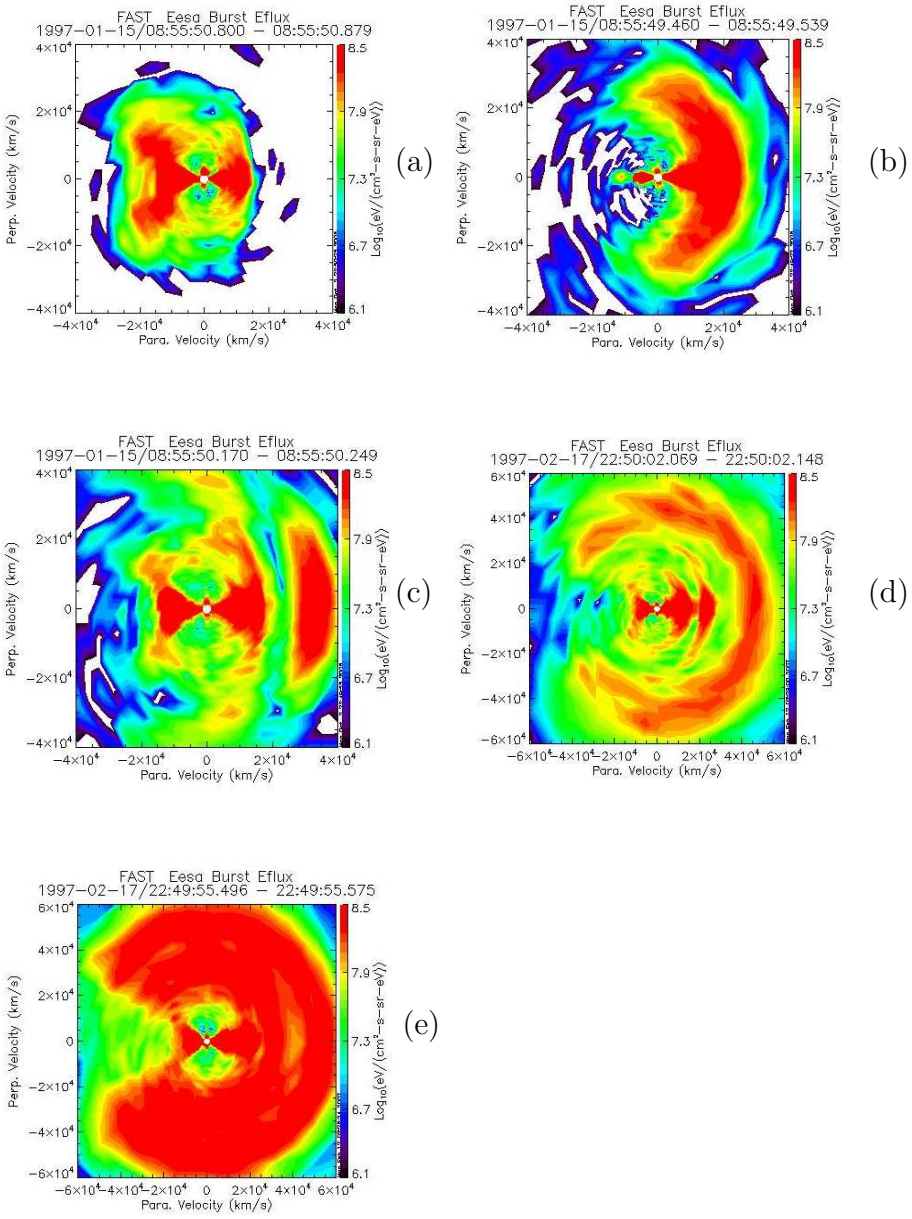


Figure 3.10. Different types of electron flux distributions. The vertical and horizontal axes represent parallel and perpendicular velocities respectively, where the downward direction always lies on the right hand side. (a) A conic distribution from 08:55:50.800 to 08:55:50.879 UT on 1997-01-15. (b) A single-shell distribution from 08:55:49.460 to 08:55:49.539 UT on 1997-01-15. (c) A double-shell distribution from 08:55:50.170 to 08:55:50.249 UT on 1997-01-15. (d) A triple-shell distribution from 22:50:02.069 to 22:50:02.148 UT on 1997-02-17. (e) A loss-cone distribution from 22:49:55.496 to 22:49:55.575 UT on 1997-02-17 .

### 3.4 The ratio of perpendicular to parallel electron number density

Inertial Alfvén waves are known to accelerate electrons in the parallel direction along the magnetic field line [Su et al.,2004; Ergunet al.,2005]. We found that the electron anisotropy $F_\perp/F_\parallel \leq 0.1$ is observed for Alfvénic acceleration events with altitudes $>\sim$ 2500 km at nightside, where $F_\perp$ and $F_\parallel$ represent the electron flux peak in the perpendicular and parallel direction, respectively. The ratio of electron flux peak $F_\perp/F_\parallel \sim 1$ is often seen in the dayside. Moreover, the parallel and perpendicular fluxes of electrons are mostly in the same magnitude at altitudes ( $<\sim$ 2500 km) at the nightside.

Electron number density measurements for Alfvénic acceleration events at altitudes $>$ 3000 km in the dayside and the nightside are shown in Tables 3.3 and 3.4, respectively. The density is the zero moment quantity which is more accurate than higher moment quantities such as velocity or temperature. Hence, we have chosen it to represent anisotropy measurements of electron distributions. In the density calculation, we restricted the electron energy within the range of $20eV - 10keV$ to exclude the photoelectron effect caused by the spacecraft charging.

The electron number densities are calculated within the region where Alfvénic perturbations were observed. The loss-cone is estimated to be $\sim 30^0$ at 3000-4000 km altitudes. The parallel electron number density ($N_\parallel$) is calculated from electrons moving in the downward direction (along the magnetic field line) with pitch angles between $-30^0$ and $30^0$ in the Northern Hemisphere, while the loss-cone electron number density ($N_{lc}$) is obtained from upward electrons with pitch angles between $150^0$ and $210^0$. The perpendicular electron number density ($N_\perp$) is obtained from the average value of densities in pitch angles $60^0 - 120^0$ and $240^0 - 300^0$. Seven events occurred in the Southern Hemisphere, which is marked by "south" in the last column of Tables 3.3-3.4. It should be noted that in the Southern Hemisphere the loss-cone is estimated between $-30^0$ and

$30^0$, opposite of that in the Northern Hemisphere. Events in the morning section between 6:00 and 8:00 MLT are excluded.

Table 3.3. Electron number density ratio at altitudes $> 3000km$ in the dayside

| Date | MLT | Period(s)/ Distance(km) | Orbit | $N_\perp/N_\parallel$ | $N_\perp/N_{lc}$ | *Note* |
|---|---|---|---|---|---|---|
| 97-03-26 | 10.7-10.8 | 30/180 | 2348 | 1.2 | 2 | South |
| 97-07-06 | 12.6 | 40/240 | 3446 | 2 | 4 | |
| 97-07-09 | 9.5-9.6 | 30/180 | 3479 | 1.5 | 2.2 | |
| 97-07-24 | 10.8-11.1 | 60/360 | 3644 | 0.8 | 1 | |
| 97-08-28 | 11.2 | 30/180 | 4020 | 3 | 6 | |
| 98-02-18 | 9 | 30/180 | 5902 | 2 | 4 | |
| 98-03-22 | 9.0-9.3 | 60/360 | 6252 | 1 | 1.7 | |
| 98-05-29 | 12.7-12.5 | 50/300 | 6992 | 1.3 | 2.2 | South |
| 98-06-10 | 10.5-10.6 | 60/360 | 7121 | 1.3 | 1.5 | South |
| 98-08-26 | 16.6-16.8 | 60/360 | 7956 | 1.5 | 2.5 | |
| 98-06-28 | 17.1-17.4 | 50/300 | 7957 | 1 | 2 | |
| 98-09-18 | 14.5-14.5 | 40/240 | 8206 | 3 | 4 | |
| 98-09-18 | 14.4-14.5 | 40/240 | 8207 | 2.5 | 4 | |
| 98-09-24 | 12.8-12.8 | 40/240 | 8267 | 2.5 | 3.7 | |
| 98-09-24 | 12.0-12.0 | 50/300 | 8275 | 1.7 | 3 | |
| 98-10-01 | 12.5 | 40/240 | 8343 | 2.5 | 3 | |
| 98-10-07 | 11.4-11.5 | 40/240 | 8414 | 2 | 3 | |
| 98-10-23 | 10.2-10.3 | 60/360 | 8587 | 0.5 | 1 | |
| 98-12-28 | 14.0-13.9 | 60/360 | 9301 | 1.7 | 2.6 | South |
| 99-02-18 | 8.9 | 30/180 | 9868 | 2 | 4 | |
| 99-04-17 | 16 | 30/180 | 10494 | 2.3 | 3.3 | |
| 99-05-18 | 14.5 | 40/240 | 10837 | 1.5 | 2 | |
| 99-09-22 | 12.9 | 30/180 | 12216 | 2.5 | 4 | |
| 99-10-21 | 10.6 | 60/360 | 12531 | 1.2 | 2.2 | |

The ratios of $N_\perp/N_\parallel$ and $N_\perp/N_{lc}$ for all 24 events are listed in the fifth and sixth columns of Table 3.3, where the mean values are 1.90 and 2.88, respectively. Electrons in the perpendicular direction may come from secondary electrons due to the ionization process in the low-altitude ionosphere. Diffusion may also play a part for trapped elec-

trons in the perpendicular direction. We seldom see AKR emissions in cases summarized in Table 3.3. AKR emissions can be seen in 6 cases, but they are very weak. No strong kilometric emission signals were recorded in the dayside.

Table 3.4. Electron number density ratio at altitudes $> 3000km$ at the nightside

| Date | MLT | Period(s)/ Distance(km) | Orbit | $N_\perp/N_\parallel$ | $N_\perp/N_{lc}$ | *Note* |
|---|---|---|---|---|---|---|
| 97-01-07 | 0.4 | 08/48 | ⋆1504 | 0.2 | 0.25 | |
| 97-01-15 | 23.8 | 40/240 | ⋆1589 | 0.2 | 0.2 | |
| 97-02-03 | 22.6 | 30/180 | 1797 | 0.3 | 0.3 | |
| 97-02-08 | 21.6 | 60/360 | 1850 | 0.5 | 0.4 | |
| 97-02-08 | 22.6 | 30/180 | ⋆1845 | 1 | 1 | |
| 97-02-13 | 22.8 | 50/300 | ⋆1906 | 0.3 | 0.3 | |
| 97-02-14 | 21.3 | 20/120 | ⋆1915 | 0.2 | 0.3 | |
| 97-02-16 | 22.7 | 30/180 | ⋆1940 | 0.5 | 0.3 | |
| 97-02-21 | 21.8 | 20/120 | 1992 | 0.5 | 0.5 | |
| 97-05-25 | 23.6 | 50/300 | 2991 | 0.5 | 1 | South |
| 97-09-15 | 0.5 | 20/120 | 4217 | 0.3 | 0.3 | |
| 97-12-17 | 22.3 | 30/180 | ⋆1952 | 0.3 | 0.3 | |
| 98-01-18 | 20.5 | 40/240 | 5570 | 0.3 | 0.3 | |
| 98-05-21 | 0.8 | 50/300 | ⋆6903 | 0.7 | 0.7 | South |
| 98-06-05 | 22.9 | 90/540 | 7066 | 0.5 | 0.5 | South |
| 99-03-09 | 6.5 | 30/180 | 10074 | 0.3 | 0.2 | |
| 99-10-02 | 0.8 | 50/300 | 12323 | 0.4 | 0.3 | |
| 99-10-27 | 21.6 | 40/240 | 12596 | 0.5 | 0.5 | |
| 99-10-30 | 22 | 40/240 | 12631 | 0.4 | 0.4 | |
| 99-11-07 | 22.3 | 50/300 | 12723 | 1 | 1.5 | |

AKR emissions occurred in 15 events listed in Table 3.4. We mark the case with a star symbol in the fourth column to indicate the short-burst event. It is difficult to isolate the discrete short burst signatures from AKR signals for the remaining 7 cases.

The ratios of $N_\perp/N_\parallel$ and $N_\perp/N_{lc}$ for all 20 cases are listed in the fifth and sixth columns in Table 3.4, where the mean values are 0.57 and 0.66, respectively. This re-

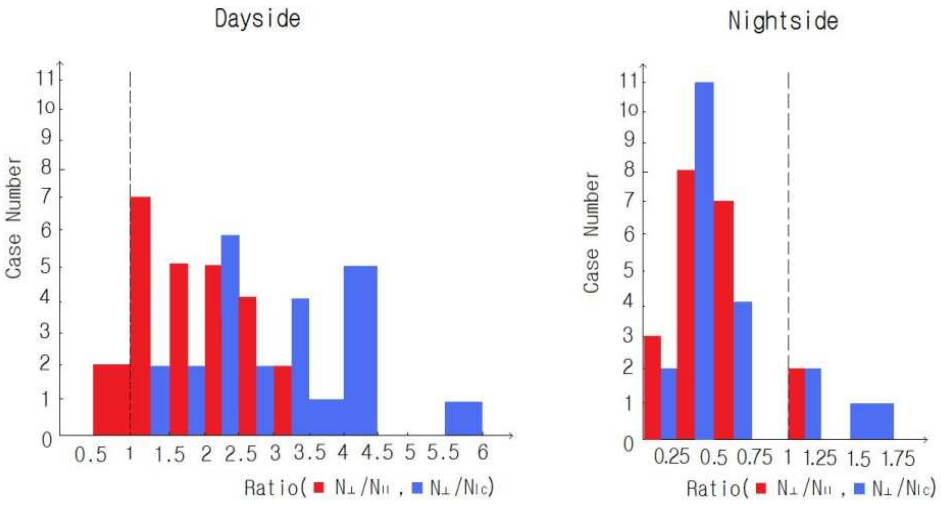


Figure 3.11. The anisotropy of electron number density in the dayside (left) and at the nightside (right).

sult confirm that counter-streaming electrons are accelerated in the parallel direction by bidirectional parallel electric fields generated from inertial Alfvén waves. [Su et al, 2004; Ergun et al., 2005].

The anisotropy of electron number density in dayside and at night is displayed in Figure 3.11, where the vertical dashed line represents $N_\perp/N_\parallel$ ( or $N_\perp/N_{lc}$) $= 1$. The red and blue bars represent the ratios of $N_\perp/N_\parallel$ and $N_\perp/N_{lc}$, respectively. For most cases, The ratio is greater than 1 in the dayside, but it is less than 1 at the nightside.

# CHAPTER 4

# SUMMARY AND DISCUSSION

Eight short burst AKR events are reported in this thesis. The event identifying method has gradually evolved to improve the screening efficiency as described in Chapter 2. Our results support the possible relation between Alfvén waves and S-burst AKR emissions suggested by Ergun et al. [2006] and Su et al. [2007]. Additionally, an interesting phenomenon of the electron density anisotropy is discovered based on detailed examination of twenty-four Alfvénic acceleration events in the dayside and twenty at the nightside.

## 4.1 Basic concepts

We introduced some basic concepts related to this research in the first chapter. They are necessary in understanding the study of the relationship between Alfvén waves and AKR emissions.

(1) Auroral Kilometric Radiation (AKR) — An intense radio emission which is believed to be generated by the electron maser instability in the auroral density cavity in the upward current region. Its frequency is similar to the local electron cyclotron frequency between 50 and 800 kHz according local magnetic fields.

(2) AKR generation mechanisms — (a) The electron cyclotron maser due to unstable electron distributions; and (b) an upward electron beam causing the upper hybrid resonance. Both mechanisms require the plasma condition of $\omega_{pe}/\omega_{ce} << 1$. The auroral density cavity in the upward current region is known to be the AKR source region.

(3) Short burst emissions — Discrete pulses of narrow-band emissions which reoccur several times within a few seconds. Alfvén waves are suggested to create unstable electron distributions, triggering electron cyclotron maser instability to generate observed short burst emissions.

(4) Alfvén waves — A low frequency MHD wave propagating along the magnetic field, with perturbations of the perpendicular electric and magnetic fields. Electrons can be accelerated by the bidirectional parallel electric fields generated by inertial Alfvén waves.

(5) Three auroral regions — There are the upward current region, the downward current region, and the polar cap boundary acceleration region. The upward current region is where down-going electrons are accelerated by the converging electric field. AKR emissions may occur in the aurora cavity in this region. The downward current region contains intense up-going accelerated electrons and down-going accelerated ions. The polar cap boundary region lies near the open-close magnetic field line boundaries where waves dominate the particle acceleration. Alfvén waves are suggested to play a significant role in this region.

## 4.2 A method in seeking S-burst AKRs

Ergun et al. [2006] and Su et al. [2007] have suggested that S-burst AKR emissions may relate to propagating Alfvén waves. A systemaic search of Earth-based short-bursts is carried out in our investigation. Three years of FAST data was examined, the screening process was gradually improved from our experiences. The final screening process is summarized below:

(1) Selected date/time when AE indices are greater than 150.

(2) Scanned summary plots of electron spectrogram and field data to identify possible Alfvénic acceleration events.

(3) Selected the orbits with altitudes higher than 2500 km, and the electron flux peak anisotropy $F_{\perp}/F_{\parallel}$ is less than 0.1 .

(4) Downloaded the data file through DM. Eliminated data size less than 60 MB per orbit (which do not contain sufficient high-resolution data).

(5) Screened plots of (a)$\delta$B; (b)$\delta$E; (c) SfaBurst V5-V8; (d) SfaAve V5-V8; (e) SfaBurst V1-V2; and (f) SfaAve V1-V2 in SDT to identify AKR emissions.

(6) Examined whether both Alfvén waves and AKR emissions are coexisted.

(7) Examined high-resolution PWT plots to identify discrete short-burst emissions.

### 4.3 Generation mechanism of S-burst AKR

AKR emissions are believed to be generated by electron maser instability associated with electron shell distributions [Pritchett, 1984a; Louarn et al., 1990; Delory et al., 1998; Ergun et al.,1998, 2000; Pritchett et al., 2002]. These distributions are found in the upward current region, where electrons are accelerated by quasi-static parallel electric fields. Ergun et al. [2006] suggested that S-bursts are associated with Alfvén waves rather than quasi-static current systems. Unstable electron distributions were observed in all eight S-burst events, such as single and multiple shells and conics, which are possible candidates in triggering electron cyclotron maser instability. Su et al. [2007] have suggested that single and multiple shell distributions as well as electron conics distributions generated by propagating Alfvén waves are the sources of S-burst AKR. Our statistic results support this idea and will benefit to the future study of S-bursts.

Based on our study, S-burst emissions are usually associated with common AKR signals. It is difficult to distinguish discrete signatures from strong AKR emissions, because the magnitude of AKRs is $1 \sim 2$ order stronger than that of S-bursts. We suggest that the probability in finding S-bursts is much higher in the Alfvénic acceleration regions than regions with quasi-static electric fields.

## 4.4 Characteristics of observed S-burst AKR emissions

All S-burst events occur at nightside during winter months. The unstable electrons move upward along the field line due to the negative drift in the power density spectrogram. A single burst travels a distance less than 60 km within 0.1-0.2 seconds. The discrete pulses usually reoccur several times within a few seconds. The reoccurrence frequency is estimated to be $\sim$ 10 Hz. The source region of emissions is estimated to be greater than 2600 km altitude.

The plasma condition $\omega_{pe}/\omega_{ce} << 1$ is necessary in triggering electron cyclotron maser instability and/or electron upper hybrid wave interaction. The density is expected to be lower at the nightside in winter compared to that at the dayside or in summer. In addition, the plasma density is expected to be lower at high altitudes ($> 2600km$) than that at low altitudes ($< 2500km$). This may explain why all events are found at high altitudes at night in winter. However, we are not able to estimate the plasma density in the source region of short burst AKR, because no event was found where the satellite flew through the source region. The plasma condition of $\omega_{pe}/\omega_{ce} << 1$ may not be easy to satisfy in the Earth's auroral enviroment compared to that in Jupiter's magnetosphere, because the electron cyclotron frequency is smaller on Earth than that in Jupiter due to Jupiter's strong magnetic field. This may explain why the occurrence frequency of Earth-based short-bursts is extremely low. Our result, eight events in three year, represents the minimum occurrence frequency.

## 4.5 Electron number density anisotropy

Twenty-four dayside Alfvénic events and twenty nightside events were examined in detail. We found that the electron number density along the magnetic field line is higher compared to that in the perpendicular direction at the nightside. Moreover, the number

density in the loss cone is comparable to that in the downward direction parallel to the magnetic field line. This result supports the idea that counter-streaming electrons are accelerated by bidirectional parallel electric fields generated from inertial Alfvén waves [Su et al.,2004; Ergunet al.,2005].

The opposite number density anisotropy was obtained in the dayside. In the dayside, $N_{\perp}/N_{lc}$ is greater than $N_{\perp}/N_{\parallel}$ indicating that that majority of electrons in the loss cone are deposited in the ionosphere. Furthermore, the density in the perpendicular direction is higher than that in the field-align direction in the dayside, which means that the secondary electrons due to ionization and trapped electrons due to diffusion may play important roles in the dayside. Different electron characteristics between nightside and dayside are the subject of future study. A major contribution of our study is to build a database for future studies in the Alfvénic acceleration regions.

## REFERENCES


1. Alexander, J. K., and M. L. Kasier (1976), Terrestrial kilometric radiation:1:Spatial structure studies, J. Geophys. Res., 81, 5948.

2. Alfvén, H. Existence of electromagnetic-hydrodynamic waves (1942), Nature, 150, 405

3. Andersson, L., R.E. Ergun, D. L. Newman, J. P. McFadden, C.W. Carlson, and Y.-J. Su (2002), Characteristics of parallel electric fields in the downward current region of the aurora, Phys. Plasmas, 9, 8, 3601.

4. Beneditkov, E.A., G. G. Getmansev, Y. A. Sazonov, and A. F. Tarasov (1965), Preliminary results of measurement of the intensity of disturbed extraterrestrial radio-frequency emission at 725 and 1525 kHz frequencies by the satellite Electron-2, Kosm. Issled., 3, 614.

5. Budden, K. G. (1986), The theory of radio windows in the ionosphere and magnetosphere. II, J. Atmospheric and Terrestrial Physics, 48, 633.

6. Budden, K. G., and D. Jones (1987), Conversion of electrostatic upper hybrid emissions to electromagnetic O and X mode waves in the earth's magnetosphere, Annales Geophysicae, 5, 21.

7. Carlson, C. W., R. F. Pfaff, and J. G. Watzin (1998a), The Fast Auroral SnapshoT (FAST) mission, Geophys. Res. Lett., 25, 2013.

8. Carlson, C. W., et al. (1998b), FAST observations in the downward auroral current region: Energetic up going electron beams, parallel potential drops and ion heating, Geophys. Res. Lett., 25, 2017.

9. Calvert, W. (1981a), The signature of auroral kilometric radiation on ISIS-1 ionograms, J. Geophys. Res., 86, 76.

10. Calvert, W. (1981b), The auroral plasma cavity, Geophys. Res. Lett., 8, 919-921.

11. Cattel, C., et al. (1998), The association of electrostatic ion cyclotron waves, ion and electron beams and field-aligned current: FAST observations of an auroral zone crossing near midnight, Geophys. Res. Lett. , 25, 2053.

12. Chaston, C. C., C. W. Carlson, W. J. Peria, R. E. Ergun, and J. P. McFadden (1999), FAST observations of inertial Alfven waves in the dayside aurora, Geophys. Res. Lett., 26, 647.

13. Chaston, C.C., C. W. Carlson, R. E. Ergun, and J. P. McFadden (2000), Alfven waves, Density Cavities and Electron Acceleration Observed from the FAST Spacecraft, Phys. Scr., T, 85, 64.

14. Chaston, C. C., J. W. Bonnell, C. W. Carlson, M. Berthomier, L. M. Peticolas, I. Roth, J. P. McFadden, R. E. Ergun, and R. J. Strangeway (2002a), Electron acceleration in the ionospheric Alfven resonator, J. Geophys. Res., 107, A11, 1413, doi:10.1029/2002JA009272.

15. Chaston, C. C., J. W. Bonnell, L. M. Peicolas, C. W. Carlson, J. P. McFadden, and R. E. Ergun (2002b), Driven Alfven waves and electron acceleration: A FAST case study, Geophys. Res. Lett., 29(11), 10.1029/2001GL013842.

16. Chaston, C. C., J. W. Bonnell, C. W. Carlson, R. J. Strangeway, J. P. McFadden, and R. E. Ergun (2003), Kinetic effects in the acceleration of auroral electrons in small scale Alfvén waves: A FAST case study, Geophys. Res. Lett. 30, 6, 1289, doi:10.1029/2002GL015777.

17. Delory, G. T., et al (1998), FAST observations of electron distributions within AKR source regions, Geophys. Res. Lett., 25, 2069.

18. Dusenbery, P. B., and L. R. Lyons (1982), General concepts on the generation of auroral kilometric radiation, J. Geophys. Res., 87, 7467.

19. Elphic, R. C., J. D. Means, R. C. Snare, R. J. Strangeway, L. Kepko, and R. E. Ergun (2001), Magnetic field instruments for the Fast Auroral SnapshoT explorer, Space Sci. Rev. 98, 151.

20. Ergun, R. E., C. W. Carlson, J. P. McFaddan, F. S. Mozer, G. T. Delory, W. Peria, C. C. Chaston, M. Temerin, R. Elphic, R. strangeway, R. Pfaff, C. A. Cattel, D. Klumpar, E. Shelley, W. Peterson, E. Moebius, and L. Kistler (1998), FAST satellite wave observations in the AKR source region, Geophys. Res. Lett., 25, 2061.

21. Ergun, R. E., C. W. Carlson, J. P. McFaddan, G. T. Delory, R. J. Strangeway, and P. L. Pritchett (2000a), Electron-cyclotron maser driven by charged particle acceleration from magnetic field-aligned electric fields, Astrophys. J., 538, 456.

22. Ergun, R. E., C. W. Carlson, J. P. McFadden, F. S. Mozer, and R. J. Strangeway (2000b), Parallel electric fields in discrete arcs, Geophys. Res. Lett., 27, 4053-4056.

23. Ergun, R. E., L. Andersson, C. W. Carlson, D. L. Newman, and M. V. Goldman (2003), Double layers in the downward current region of the aurora, Nonlinear Process in Geophysics, 10, 45-52.

24. Ergun, R. E., L. Andersson, Y.-J Su, D. L. Newman, M. V. Goldman, C. C. Chaston, and C. W. Carlson (2005), Localized parallel electric fields associated with inertial Alfvén waves, Physics of Plasmas 12, 072901.

25.Ergun, R. E., Y.-J. Su, L. Andersson, F. Bagenal, P. A. Delemere, R. L. Lysak, and R. J. Strangeway (2006), S-burst and Jupiter ionospheric Alfvén resonator, J. Geophys. Res., 111, A06212, doi:10.1029/2005JA011253.

26. Frank, L. and Ackerson, K.(1971), Observations of charged particle precipitation into the auroral zone, J. Geophys. Res., 76, 3612-3643.

27. Gurnett, D., (1972), Electric field and plasma observations in the magnetosphere, in Critical problems of magnetospheric physics, edited by E. Dyer, pp. 123-138, National Academy of Sciences, Washington D.C., 1972

28. Gurnett, D.A. (1974), The Earth as a radio source: Terrestrial kilometric radiation, J. Geophys. Res., 79, 4227-4238.

29. Gurnett, D. A., and J. L. Green, On the polarization and origin of auroral kilometric radiation (1978), J. Geophys. Res., 83, 689-696.

30. Hilgers, A. (1992), The auroral radiating plasma cavities, Geophys. Res. Lett., 19(3), 237-240.

31. Hwang, K.J., K. A. Lynch, C. W. Carlson, J. W. Bonnell, and W. J. Peria (2006a), Fast Auroral Snapshot observations of perpendicular DC electric field structures in downward auroral current regions: Morphology, J. Geophys. Res., 111, A09205, doi:10.1029/2005JA011471.

32. Hwang, K.J., K. A. Lynch, C. W. Carlson, J. W. Bonnell, and W. J. Peria (2006b), Fast Auroral Snapshot observations of perpendicular DC electric field structures in downward current regions: Implications, J. Geophys. Res., 111, A09206, doi:10.1029/2005JA011472.

33. Kaiser, M. L., J. K. Alexander, A. C. Riddle, J. B. Pearce, and J. W. Warwick (1978), Direct measurements by Voyagers I and 2 of the polarization of terrestrial kilometric radiation, Geophys. Res. Lett., 5, 857-860.

34. Keiling, A., J. R. Wygant, C. Cattell, M. Johnson, M. Temerin, F. S. Mozer, C. A. Kletaing, J. Scudder, and C. T. Russell (2001), Properties of large electric fields in the plasma sheet at 4-7 RE measured with Polar, J. Geophys. Res., 106, 5779.

35. Keiling, A., J. R. Wygant, C. A. Cattell, M. Johnson, F. S. Mozer, and C. T. Russell (2003), The global morphology of wave Poynting flux: Powering the aurora, Science, 299, 383.

36.Kletzing, C. A., Electron acceleration by kinetic Alfvén waves (1994), J. Geophys. Res., 99, 11, 095.

37. Knudsen, D. J., M. C. Kelley, G. D. Earle, J. F. Vickrey, and M. Boehm (1990), Distinguishing Alfven waves from quasi-static field structures associated with the discrete aurora: Sounding rocket and HILAT satellite measurements, Geophys. Res. Lett., 17, 921.

38. Kraus, J.D. (1956), Some observations of the impulsive radio signals from Jupiter, Astro. J., 61, 182.

39. Kurth, W.S., Baumback, M. M., Gurnett, D.A. (1975), Direction finding measurements of auroral kilometric radiation, J. Geophys. Res., 80, 2764.

40. Kumamoto, A., and H. Oya, Asymmetry of occurrence-frequency and intensity of AKR between summer polar region and winter polar regionsources (1998), Geophys. Res. Lett, 25, 2369.

41. Lysak, R. L. and Y. Song (2003), Kinetic theory of the Alfvén wave acceleration of auroral electrons, J. Geophys. Res., 108, NO. A4, 8005, doi:10.1029/2002JA009406.

42. Louarn, P. A., Roux, H. de Feraudy, D. Le Queau, M. Andre, and L. Matson (1990), Trapped electrons as a free energy source for the auroral kilometric radiation, J. Geophys. Res., 95, 5983.

43. Lundin, R., G. Haerendel, and S. Grahn (1994), The Freja science mission, Space Science Reviews, 70, 405, 1994, doi:10.1007/BF00756879.

44. Mellott, M. M., W. Calvert, R. L. Huff,and D. A. Gurnett (1984), DE-1 obsevations of ordinary mode and extraordinary mode auroral kilometric radiation, Geophys. Res. Lett., 11, 1188.

45. Melrose, D. B. and G. A. Dulk (1982), Electron-cyclotron masers as the source of certain solar and stellar radio bursts, Astrophys. J., 259, 844.

46. Pritchett, P. L. (1984a), Relativistic dispersion and the generation of auroral kilometric radiation, Geophys. Res. Lett., 11, 143.

47. Pritchett, P. L. (1984b), Relativistic dispersion, the cyclotron maser instability and kilometric radiation, Geophys. Res. 89, 8957.

48. Pritchett, P. L., and R. J. Strangeway (1985), A simulation study of kilometric radiation generation along an auroral field line, J. Geophys. Res., 90, 9650.

49. Pritchett, P. L., R. J. Strangeway, R. E. Ergun, and C. W. Carlson (2002), Generation and propagation of cyclotron maser emission in the finite AKR source cavity, J. Geophys. Res., 107(A12), 1437, doi:10.1029/2002JA009403.

50. Strangeway, R. J., L. Kepko, R. C. Elphic, C. W. Carlson, R. E. Ergun, J. P. McFadden, W. J. Peria, G. T. Delory, C. C. Chaston, M. Temerin, C. A. Cattell, E. Mobius, L. M. Kistler, D. M. Klumpar, W. K. Peterson, E. G. Shelley, and R. F. Pfaff (1998), FAST observations of VLF waves in the auroral zone:evidence of very low plasma densities, Geophys. Res. Lett., 25, 2065.

51. Strangeway, R. J., R. E. Ergun, C. W. Carlson, J. P. McFadden, G. T. Delory, and E. L. Pritchett (2001), Accelerated electrons as the source of auroral kilometric radiation, Phys. Chem. Earth, 26, 1-3, 145-149.

52. Strangeway, R. J., R. E. Ergun, Y.-J. Su, C. W. Carlson, and R.C. Elphic (2005), Factors controlling ionospheric outflows as observed at intermediate altitudes, J. Geophys. Res., 110, A03221, doi:10.1029/2004JA010829.

53. Su, Y.-J., R. E. Ergun, W. K. Peterson, T. G. Onsager, R. Pfaff, C. W. Carlson, and R. J. Strangeway (2001), Fast Auroral SnapshoT observations of cusp electron and ion structures, J. Geophys. Res., 106, 25, 595.

54. Su, Y.-J., S. T. Jones, R. E. Ergun, and S. E. Parker (2004), Modeling of field-aligned electron bursts by dispersive Alfven waves in the dayside auroral region, J. Geophys. Res., 109, A11201, doi:10.1029/2003JA010344.

55. Su, Y.-J., R. E. Ergun, S. T. Jones, R. J. Strangeway, C. C. Chaston, F. Bagenal, S. E. Parker, and J. L. Horwitz (2007), Generation mechanism of short-burst radiation in an Alfvenic acceleration region, J. Geophys. Res., In press.

56. Thompson, B. J., and R. L. Lysak, Electron acceleration by inertial Alfvén waves (1996), J. Geophys. Res., 101, 5359.

57. Wang, X.-Y, J.-S. Wu, Y. Li, S. Wang, J.-K. Zhao, J.-B. Cao (2002), Alfven waves in regions of magnetic reconnection and the acceleration of newborn ions, Chinese Astronomy and Astrophysics, Volume 26, Issue 1, p. 29-39.

58. Wu, C. S., and L. C. Lee (1979), A theory of the terrestrial kilometric radiation, Astrophy. J., 230, 621.

59. Winglee, R. M., and P. L. Pritchett (1986), The generation of low-frequency electrostatic waves in association with auroral kilometric radiation, J. Geophys. Res., 91, 13531.

60. Wygant, J. R., et al.(2000), Polar spacecraft based comparison of intense electric fields and pointing flux new and within the plasma sheet-tail lobe boundary to UVI images: An energy source for the aurora, J. Geophys. Res., 105, 18, 675.

## BIOGRAPHICAL INFORMATION

Lun Ma received his Bachelor of Science in Physics from Shaanxi Normal University in 1993. He received his Master of Science in Physics from the University of Texas at Arlington in May 2007.